Schwartz  N 62  14601

RESEARCH
LABORATORIES

UNITED AIRCRAFT CORPORATION

RESEARCH

# UNITED AIRCRAFT CORPORATION
# RESEARCH LABORATORIES
## EAST HARTFORD, CONN.

Report R-2297-1

Mission Capabilities of Ion Engines
Using SNAP-8 Power Supplies
Contract NAS5-935
Phase I - Summary Report

UNCLASSIFIED

T. N. Edelbaum

W. R. Fimple

F. W. Gobetz

H. S. London

APPROVED BY C. Oickle

C. Oickle
Head, Evaluation Section

**NO. OF PAGES** 72

**DATE** August 1961

Report R-2297-1

## Mission Capabilities of Ion Engines

## Using SNAP-8 Power Supplies

Contract NAS5-935
Phase I - Summary Report

TABLE OF CONTENTS

TABLE OF CONTENTS
(contd.)

Report R-2297-1


Mission Capabilities of Ion Engines

Using SNAP-8 Power Supplies

Contract NAS5-935
Phase I - Summary Report

SUMMARY

/4601 Mission performance capabilities of ion engines powered by the 30 kw and
60 kw SNAP-8 power supplies are compared for the following missions: a 24-hr
equatorial satellite, a 100 n mi lunar satellite, a 500 n mi Mars satellite, a
Mercury probe, and an out-of-the-ecliptic probe. The capabilities of arc-jet
engines and chemical engines for the same missions are compared with those of
the ion engines. The majority of the comparisons are for 8500-lb spacecraft
which are boosted into a 300 n mi orbit by the Atlas-Centaur. Variations in
initial orbit altitude, the use of actual launch dates rather than dates based
on simplifying assumptions, and the combined use of chemical and electrical pro-
pulsion systems were also evaluated in terms of their effect on mission per-
formance.

CONCLUSIONS


1. For payloads below about 4500 lb, spacecraft with ion engines powered
by the 60 kw SNAP-8 can perform all the specified missions in a shorter time than
those powered by the 30 kw SNAP-8. For payloads larger than 4500 lb, the 30 kw
system provides shorter flight times. However, this latter area of superiority
is primarily of academic interest since the flight times tend to be prohibitively
long with either system.

2. The payload capability of arc-jet propulsion will be limited by the
maximum attainable specific impulse. For any given specific impulse, spacecraft
powered by the 30 kw SNAP-8 can carry about 1000 lb more payload than spacecraft
powered by the 60 kw SNAP-8 at the expense of doubling the flight time. Since
the flight times for arc-jets with either power supply tend to be a small fraction
of the nominal 10,000 hr (417 day) power supply lifetime, this flight time penalty
is of minor significance, and the 30 kw system is therefore the preferable size
for use with arc-jet engines.

3. Spacecraft with arc-jet engines can perform the 24-hr and lunar satellite missions in a shorter time than those with ion engines but cannot carry as much payload. Arc-jet spacecraft are incapable of performing the missions to Mars, to Mercury, or out of the ecliptic plane.

4. For the 24-hr and lunar satellite missions, the ion-engine spacecraft can carry more payload than spacecraft with chemical rockets and, in addition, can make available large amounts of power in the final orbit. However, a large time penalty is involved in the use of the ion engine.

5. For the Mars satellite mission, the Mercury flyby, and the out-of-the-ecliptic mission, the chemical-rocket spacecraft can carry about as much payload as spacecraft powered by ion rockets and in a shorter time. However, the large available power of the ion engine power supply would allow the performance of scientific experiments which could not be conducted if the chemical rocket were used.

6. The use of chemical and ion propulsion in combination is promising for some of the more ambitious missions and should be examined further. For many missions, vehicles with the combined propulsion system can carry more payload in a shorter time than those with ion propulsion only, but the difference in specific cases may not be large.

## RECOMMENDATIONS

1. Development of the 60 kw SNAP-8 power supply should be continued for use in ion-engine-powered spacecraft. Although chemical propulsion appears competitive with this ion propulsion system for interplanetary missions, development of the ion system and attendant space tests of the vehicle would provide experience for later high-performance electrically-propelled spacecraft and would also allow the performance of scientific experiments in space which are otherwise not feasible.

2. Development of the 30 kw SNAP-8 power supply should be continued for use with an arc-jet for near-Earth missions. This propulsion system would provide large amounts of electrical power in the 24-hr equatorial orbit and would enable the early realization of such practical applications as high-quality, large-capacity television relays and high-quality image transmission from orbiting astronomical telescopes.

## INTRODUCTION

The ion engine is one of the most promising propulsion methods for use in spacecraft, after they have been placed in a low-altitude orbit by a high-thrust booster. Ion propulsion appears to provide the only feasible means of performing ambitious space missions, the fastest method of performing moderately ambitious missions, and the most economical method of raising large power supplies into high-altitude Earth orbits. This last application results from the fact that the power supply for the engine can be used for other purposes after the orbit has been established. This feature would also have application to interplanetary missions where the entire power supply output would be available during coast periods or at the end of missions which terminate in orbit around other planets.

The studies reported herein were performed for NASA Headquarters under Contract NAS5-935 to provide quantitative comparisons of ion propulsion with other propulsion systems. First-generation systems currently under development have been considered in Phase I of this study, the results of which are presented herein. Later high-performance systems will be considered in Phase II. The primary interest in Phase I was applications of the 30 kw and 60 kw SNAP-8 power supplies to NASA missions scheduled for the 1965 to 1970 time period.

## SCOPE AND METHOD OF ANALYSIS

### Missions

Because the thrust of ion propulsion systems is very much smaller than the weight of these systems, they may be used only after an orbit has been established. For the purposes of this study, the ion-propelled spacecraft are generally assumed to be placed into a 300 n mi circular orbit by an Atlas-Centaur booster. The performance of the ion-propelled spacecraft is compared with the performance of chemically-propelled and arc-jet-propelled spacecraft launched by the same booster and starting from the same orbit.

Five different missions which originate in a 300 n mi orbit are considered. These are: transfer to a 24-hr equatorial orbit, transfer to a 100 n mi lunar orbit, transfer to a 500 n mi Mars orbit, a probe passing close by Mercury, and a probe to a celestial latitude 15 deg above the ecliptic plane. The trajectories used for each of these missions are discussed briefly under each mission and in more detail in the Appendixes. The payload and time comparisons for these five missions constitute the major results of this study; however, three additional items are examined to determine their possible effect on vehicle performance:

(1) the use of higher initial orbit altitudes for the 24-hr satellite, (2) the use of actual launch dates and the actual eccentricity and inclination of Mercury's orbit for the Mercury probe, and (3) the use of chemical and electrical propulsion in combination for the out-of-the-ecliptic mission.

## Engine Efficiency

The amount of fuel necessary for an electric propulsion vehicle to perform a given mission is primarily dependent upon the specific impulse of the engine, where specific impulse is defined as the ratio of thrust to the weight flow rate of material fed into the engine. Because ion accelerators are not temperature limited, they may be operated at as high a specific impulse as is desired. However, operation at high specific impulse involves a time penalty. While the fuel weight for an electric propulsion mission is primarily dependent on the specific impulse, the time for the mission is primarily dependent upon the thrust. Equation (1) shows the dependence of the thrust upon the over-all engine efficiency, $\eta$, the input power $P$, and the specific impulse $I$.

$$F = \frac{2\eta P}{Ig} \tag{1}$$

For any given efficiency and power input the thrust is inversely proportional to the specific impulse so that the higher the specific impulse, the smaller the thrust and the longer the flight time. At the same time, an increase in specific impulse decreases fuel consumption and increases payload for a given vehicle weight so that time may be traded for payload and vice versa.

In practice the engine efficiency is usually a function of specific impulse for ion rockets, arc-jets, or any other form of electric propulsion. For ion rockets the efficiency is often broken down into two parts, a power efficiency and a propellant utilization efficiency. A useful approximate equation for the variation of power efficiency with specific impulse may be derived for ion engines by assuming that all the losses occur in the ionizer and virtually none occur in the acceleration system. This expression for power efficiency, representing the losses due to each ion that is accelerated, is given by Eq. (2) where $L$ is assumed constant for a given type of ion engine. The constant $L$, which is defined by Eq. (2), may be interpreted as the specific impulse at which power efficiency is 50%.

$$\eta_P = \frac{1}{1 + \frac{L^2}{I^2}} \tag{2}$$

The second part of the efficiency is the propellant utilization efficiency, and is defined as the ratio of the weight of propellant that is accelerated to the total weight flow of propellant. The over-all efficiency is given by Eq. (3) and represents the contribution of both the utilization efficiency and the power efficiency.

$$\eta = \frac{\eta_U}{1 + \frac{L^2}{\eta_U^2 I^2}}$$

The efficiencies assumed for the ion engines that are considered in this study are shown in Fig. 1 as a function of specific impulse. The curve for the bombardment ion engine corresponding to the configuration being developed at the NASA Lewis Research Center is based on a loss of 1000 electron volts per mercury ion and 80% propellant utilization. The curve for the cesium engine applies to a surface-contact engine of the type being developed by Hughes Aircraft Company and is based on their estimates (Ref. 1) of 20 ma/cm² ion source current, 40% heater efficiency for the ionizer, and a neutralizer power requirement which is 25% of that for the ionizer. A 95% propellant utilization has been assumed for the Hughes engine. The lowest specific impulse shown for each engine is the one at which maximum thrust is obtained for a given power input. As specific impulse is decreased below this value, the efficiency will decrease more rapidly than the specific impulse so that the thrust will actually be reduced. This maximum thrust point represents the minimum specific impulse for which an ion engine should be used. By substituting Eq. (3) into Eq. (1) and differentiating, it can be shown that maximum thrust occurs when

$$I = \frac{L}{\eta_U} \tag{4}$$

and

$$\eta = \frac{\eta_U}{2} \tag{5}$$

With 60 kw of input power the maximum thrust of the bombardment engine is 0.435 lb at a specific impulse of 2540 sec, while the maximum thrust of the cesium engine is 0.318 lb at a specific impulse of 4120 sec. At specific impulses below about 7000 sec the efficiency of the reference bombardment engine is superior to that of the reference cesium engine, while the reverse is true at specific impulses above 7000 sec.

Figure 2 shows the assumed efficiency for a hydrogen-fueled arc-jet engine. The theoretical curve is based on uniform, one-dimensional, frozen flow through a 100:1 area ratio nozzle from a chamber pressure of 1 atmosphere with a 98% velocity coefficient. It is assumed that propellant is expelled only through the exhaust nozzle and that full regenerative cooling of the entire engine can be achieved. Furthermore this regenerative cooling is assumed to be possible

with hydrogen in either a liquid or a gaseous state so that the propellant which has been vaporized in the tanks may be utilized in the engine. The fact that most of the cooling capacity of hydrogen is due to its large heat capacity and low initial temperature rather than its heat of vaporization makes this assumption reasonable.

The experimental curve is based upon recent data for hydrogen obtained by AVCO (Ref. 2). These data were apparently obtained with a nozzle area ratio smaller than 100:1 and represent an engine which is radiation cooled, so that all of the theoretical assumptions are not satisfied. In spite of the additional losses this should entail, the experimental curve has a higher efficiency than the theoretical curve at the high specific impulses. Reference 2 suggests a number of reasons that may be responsible for this difference between experimental and theoretical results, possibly the most important of which is the nonuniformity of the flow in the actual engine.

The difference between the theoretical and experimental efficiency curves can have a large effect on the comparative mission performance of the 30 kw and 60 kw power supplies. In general it is necessary to use realistic efficiency estimates if valid comparisons of power supply capability are to be obtained. However, it will be shown that in the particular case of the arc-jet a choice of the more desirable power supply is independent of which of the arc-jet efficiency curves is utilized.

The efficiency of the ion engines is compared to the efficiency of the arc-jet engines in Fig. 3. There is a specific impulse region between the two engine types where neither one can operate satisfactorily. If other types of electrical propulsion engines can be developed to operate with reasonable efficiency in this regime they may be useful for various missions with the SNAP-8. Later power supplies, which will probably have much lower specific weights than the SNAP-8, will probably tend to emphasize specific impulses above 4000 sec where the ion engine becomes efficient.

## Spacecraft Weights

The spacecraft that the Atlas-Centaur places into a 300 n mi orbit is assumed to weigh 8500 lb. This gross weight consists of eight different component weights: structure, propellant tankage, propellant insulation, residual and reserve propellant, engine, power supply, propellant, and payload. The propellant is calculated as the amount needed to perform this mission plus the amount boiled off. Propellant boil-off is considered only for the hydrogen-oxygen chemical rocket as the ion rockets do not use cryogenic propellants and the arc-jet is assumed to utilize propellant boil-off in the engine. The weight assumptions for each of the other items are listed in Table I, the insulation

weight being determined by the methods of Appendix VI. The payload weight is defined as the difference between the gross weight and the seven other component weights. This definition implies that guidance equipment and other electronics as well as the scientific experiments are included in the payload. The payload may thus be considered to include all items except the structure and propulsion system of the spacecraft.

When an electric propulsion power supply is carried, this power supply is not considered part of the payload even though it would probably constitute the power source for the payload. When such a power supply is not carried (in the chemical rocket spacecraft) the payload will necessarily have to include a power supply.

Typical weight breakdowns for several vehicles are listed in Table II.

## DISCUSSION OF RESULTS

### 24-Hr Equatorial Satellite Mission

The Atlas-Centaur is assumed to place the spacecraft in a 300 n mi orbit by means of a due-east launch from the Atlantic missile range. As the orbital altitude is raised to the 24-hr altitude, it is necessary to decrease the inclination of the orbit to the equator from its initial value of 28.5 deg down to zero. The optimum method of simultaneously changing altitude and inclination for this mission has been derived in Ref. 3, and this maneuver is used herein. The use of this optimum maneuver produces about a 20% saving in time and fuel when compared to first going out to the 24-hr orbit and then changing the inclination.

The payload capability of spacecraft with the bombardment ion engine for the 24-hr satellite mission is shown in Fig. 4 for each of the SNAP-8 powerplants. The different points on the curves represent ion engines having different specific impulses so that as specific impulse is increased, the payload and the flight time are usually increased. The solid curves represent payload as defined in the previous section, whereas the dashed curves represent the inclusion of the power supply in the definition of the payload. These dashed curves are intended primarily to facilitate the use of other assumptions for power supply weight than the ones used herein. As shown in Table I, the 60 kw power supply was assumed to weigh 3000 lb while the 30 kw power supply was assumed to weigh 2000 lb.

With the bombardment-type ion propulsion system, the 24-hr orbit can be established in a minimum time of about 120 days with 60 kw or in about 240 days

7

with 30 kw. In each case the minimum flight time corresponds to the specific impulse for maximum thrust of about 2500 sec. With either system quite large payloads can be placed into the 24-hr orbit in addition to the weight of the power supply. For example, the 60 kw system could be used to place about 4000 lb in this orbit in about 150 days and still allow about 270 days of the nominal 10,000 hr operating life of the powerplant for communications or other purposes. For very long flight times the lower weight of the 30 kw power supply causes its payload capability to become greater than that of the 60 kw system. However, if the power supply is considered to be part of the payload, the 60 kw system is superior for all flight times. In conclusion it can be said that for payloads below about 4500 lb, the 60 kw system will always supply shorter flight times. The reverse is true for payloads above 4500 lb, but these involve such long flight times that they are primarily of academic interest.

Figure 5 presents a comparison of the bombardment ion engine and the cesium ion engine for the 24-hr satellite mission. While the assumed cesium engine is superior to the assumed bombardment engine for long flight times, the difference is never very great and the bombardment engine generally appears to be preferable on a mission performance basis for these fairly heavy power supplies. Accordingly, the bombardment engine was used for the remaining missions considered.

The effect of changing initial orbit altitude on the payload that can be placed into a 24-hr orbit is illustrated in Fig. 6 for the 60 kw SNAP-8 power supply. The Atlas-Centaur is assumed as the booster in each case. With this figure it can be shown that the ion engine, by virtue of its high specific impulse, is superior to chemical rockets for increasing orbit altitude. Initial orbit altitude is a measure of the degree to which the chemical and ion engines are used in performing the 24-hr orbit mission; the higher the initial orbit altitude, the greater the utilization of the chemical system. Since Fig. 6 illustrates that payload increases with decreasing initial orbit altitude, it is apparent that the ion engine is the better system for this purpose. This figure can also be used to estimate decreases in payload capability that would be required if nuclear safety requirements dictate high launch altitudes.

Similar results for the 30 kw system and the envelope of the results for the 60 kw system are shown in Fig. 7. A comparison of these results shows that the 60 kw system is always superior to the 30 kw system for payloads below about 4500 lb. However, if the launch altitude were restricted to higher levels such as 500 n mi, the payload at which this cross-over occurs would decrease to a value such as 3500 lb.

Figure 8 shows the capability of the arc-jet engine for the same 24-hr equatorial satellite mission. Here the difference in the efficiency curves creates a large difference in the resulting times and, in particular, the slopes of the curves. However, the important point is that the arc-jet will probably be a system which is fairly limited in specific impulse no matter

which efficiency curve is considered. The 30 kw system can always carry appreciably more payload than the 60 kw system although it will require somewhat more time to do this. Since the times required to perform this mission with the arc-jet are a relatively small portion of the total lifetime of the SNAP-8, this larger time penalty is not too significant and the 30 kw system does appear to be preferable.

A summary of the arc-jet and ion engine capabilities for this mission is shown in Fig. 9. It can be seen that while the arc-jets are capable of performing this mission more rapidly than the ion engines, the latter carry appreciably more payload.

The final summary of the 24-hr equatorial satellite mission is shown in Fig. 10 where the electric propulsion systems are compared with chemical propulsion systems. The two points labeled Saturn C-1 and Centaur represent the payloads (including guidance system) that can be placed into a 24-hr orbit with these boost vehicles alone. The Saturn C-1 assumed herein is a three-stage version. The point labeled Centaur plus chemical engine represents the use of a specially designed hydrogen-oxygen chemical spacecraft on top of the Atlas-Centaur so as to increase the payload that can be placed into this orbit with chemical propulsion. However, even the arc-jet engines which are launched by the same launch vehicle can place as much payload into the orbit as can the chemical rocket and in addition can orbit the very useful 30 kw power supply. None of the chemically-propelled vehicles are capable of placing both the SNAP-8 and any useful payload into the 24-hr orbit.

## Lunar Satellite Mission

The establishment of a lunar satellite with the low-thrust propulsion systems involves a gradual spiral away from the initial orbit until the vicinity of the Moon is reached. There will generally follow a relatively short coast period and the vehicle will then spiral into the final 100 n mi circular orbit about the Moon. A detailed study of such trajectories was reported in Ref. 4, and these trajectories have been used in the present study. Figure 11 presents the performance of the bombardment ion engine for a lunar satellite mission. The results are quite similar to those for the 24-hr Earth orbit although the payloads are somewhat smaller and the flight times are somewhat longer. Once again the specific impulse of 2500 sec yields the minimum flight time while an increase in specific impulse will increase both the payload and the flight time. Figure 12 presents the corresponding capabilities of the arc-jet for the lunar satellite mission (assuming the theoretical efficiency). The relative performance with the theoretical and experimental efficiencies would be similar to that for the 24-hr mission. As with the ion engine the increased difficulty of this mission causes the flight times to increase and

the payload to decrease relative to the 24-hr orbit. The 60 kw system now has a relatively small payload capability and it is necessary to use the 30 kw system to establish appreciable payloads in the lunar orbit.

A comparison of the lunar mission capabilities of the arc-jet engines and the bombardment ion engines is shown in Fig. 13. This figure again shows that the 30 kw powerplant appears to be preferable for use with the arc-jet, while the 60 kw powerplant appears to be preferable for use with the ion rocket. Figure 14 is a summary and comparison of chemical propulsion with electric propulsion for the lunar mission. When compared to the 24-hr satellite mission, the lunar satellite mission requires slightly less fuel with chemical engines, but requires more fuel and more time with ion or arc-jet engines. In spite of this, the electrical systems are still the only methods of carrying any payload in addition to the 30 kw or 60 kw power supply into lunar orbit.

## Mars Satellite Mission

Performance of the Mars satellite mission with the ion-engine-powered spacecraft involves an initial spiral away from the Earth until the edge of the Earth's sphere of influence has been reached. Tangential thrust is essentially optimum for this portion of the mission and the generalization to the constant-thrust case in Ref. 5 of the constant-acceleration analysis reported in Ref. 6 has been used for this phase as well as for the final spiral into Mars. Once out of the Earth's sphere of influence the vehicle may be assumed to move under the primary attraction of the Sun, and it is necessary to determine an optimum transfer in the Sun's gravity field. With constant thrust, calculations have shown that this transfer will generally involve an initial thrust phase followed by a coast, followed by another thrust phase. A simple approximation to the optimum steering program for this phase of the mission that was originated at the Lewis Research Center has been utilized for this study. During the initial thrust phase, the thrust vector is assumed to make a constant angle outward from the circumferential direction. Then after the coast phase when the thrust is turned on again, the thrust vector makes an equal and opposite angle with the circumferential direction, being directed inward toward the Sun. The vehicle then enters Mars sphere of influence and spirals down to the final 500 n mi Mars orbit. Ion propulsion is attractive for this mission because it allows a complete mapping of the radiation belts of Mars while spiralling down to the final orbit altitude.

Both the Earth and Mars are assumed to have circular orbits lying in the same plane for the purposes of this analysis. This assumption greatly simplifies the analysis without appreciably affecting any propulsion system comparisons. It is assumed that the vehicle may always be launched at the time of year which will provide the maximum payload capability for the assumed flight time. The

effect of considering actual launch dates would be to restrict the allowable
launch times to a fairly narrow band for each flight time. An example of this
will be shown for the Mercury probe. In practice, the eccentricity of Mars'
orbit will increase the amount of payload that can be carried to Mars in some
years and will decrease it in other years, while the inclination of Mars' orbit
will have relatively little effect on the propulsion requirements (Ref. 7). The
use of the circular orbit may be considered to represent an average capability
during an average year.

The payload that can be placed in the final Mars orbit with the bombardment
ion engines is shown in Fig. 15. The 60 kw power supply can carry about 1000 lb
into a low-altitude Mars orbit within the nominal 10,000 hr (417 day) operating
lifetime of the powerplant. The 30 kw powerplant cannot perform this mission
unless flight times longer then the nominal operating life are considered. Each
curve represents the envelope of a number of trajectory calculations for different
specific impulses and trajectory parameters and represents an optimum coast time
for the particular assumed engine efficiency. A corresponding figure for the
arc-jet has not been prepared because the arc-jet is not capable of performing
this fairly difficult mission. The low specific impulse of the arc-jet necessitates
the use of more fuel than can be carried in a 8500-lb SNAP-8-powered stage even if
the hydrogen boil-off during the long coast periods were neglected. The arc-jet
is also incapable of performing the Mercury flyby and out-of-the-ecliptic missions
for the same reason.

Figure 16 is a comparison of a chemical rocket spacecraft and the ion engine
spacecraft for the Mars satellite mission. The Saturn and Centaur launch vehicles
are not considered for this mission as they would need considerable modification
to prevent prohibitive propellant boil-off during the transfer to Mars. The
chemical spacecraft has separate, well-insulated tankage for the propellants
that are carried to Mars; allowance is made for the weight of insulation and
for the propellant that is boiled off. If the power supply is limited to its
nominal 417-day operating life, the ion engine vehicle can carry about the same
payload as the chemical vehicle. However, it should be realized that much
information could be radioed back to Earth while the ion rocket is spiralling
down to its final orbit around Mars. Once again, if large powers are desired
for nonpropulsive purposes such as communication, electric propulsion appears
to be the only feasible way of performing the mission.

Mercury Probe Mission

As an illustration of the effects of launch dates and of the eccentricity
and inclination of a planetary orbit, the calculations for the Mercury probe
have considered all of these effects. Mercury is an interesting planet to use
for this type of analysis because its orbit has the highest eccentricity and

inclination of any planet but Pluto, and its short period of revolution creates rapidly changing launch requirements. All of the Mercury probe calculations were carried out for launch dates in the year 1968 during which Mercury makes approximately four revolutions.

A typical Mercury probe trajectory would start with a tangential thrust escape spiral from the Earth until the edge of the Earth's sphere of influence was reached. At this time, when the vehicle starts to move in heliocentric space, the thrust vector would be turned so that it tends to oppose the direction of motion of the spacecraft and to decrease its energy. As a simplifying approximation, the angle the thrust vector makes with the radius vector and with the plane of the Earth's orbit has been kept constant during this heliocentric part of the trajectory. It should be realized that the optimization of this phase of the trajectory should increase the payload that can be carried with the ion rocket and will increase the number of days during which launches are allowable.

The payload that can be carried with the 60 kw ion rocket is shown as a function of launch date in Fig. 17. These curves, along which trip time and specific impulse are approximately constant, show the variation of payload with launch date. For each date the specific impulse yielding the greatest payload was chosen unless the required trip time exceeded the expected power supply lifetime of 10,000 hrs (417 days). These results show that launch may not take place during almost the entire first half of 1968 and that there exist only two time periods, late August and mid-September, when payloads above 2000 lb may be carried. However in spite of the rapid revolution of Mercury about the Sun, it is still possible to have firing windows which are four weeks or even more in length.

Corresponding results for high thrust are shown in Fig. 18, also as a function of launch date and trip time. Both sets of results are compared in Fig. 19. It should be noted that the launch date which yields maximum payload for the chemical rocket tends to occur somewhat later in the year than that for the ion engines. The reason for this is that Mercury is approached at about the same position with either propulsion system, but the electrical propulsion system must start earlier because of its longer flight time. The maximum payload that can be carried with the chemical rocket is somewhat smaller than can be carried with the ion rocket and does not include the large power supply that the ion rocket makes available. However, trip times for maximum payload with the ion rocket are about 314 days while those for the chemical rocket are about 120 days. Figure 19 also illustrates that both systems are about equally sensitive to the effects of changes in launch date. This may be due partially to the limitations of the low-thrust trajectory analysis for the ion rocket. It is expected that later high-performance electric propulsion systems will have wider firing windows than will chemical rockets as well as greater payload capability.

12

## Out-of-the-Ecliptic Probe

The final mission to be considered is a probe which reaches a celestial latitude 15 deg above the ecliptic plane. The trajectories for the ion rocket for this mission consist of an initial spiral away from the Earth until the edge of the sphere of influence has been reached, following which the thrust is directed normal to the ecliptic plane as the vehicle moves into heliocentric space. The analyses of Ref. 8 and Appendix IV show that under such a thrust force, the vehicle will describe a small circle on the surface of an imaginary sphere of the radius of the Earth's orbit. The thrust-weight ratio of the ion engine will determine how high a latitude this small circle can reach. In cases where the vehicle must spend more than half a year revolving about the Sun, it is desirable to reverse the direction of thrust at an optimum position which is derived in Appendix IV. The thrust is assumed to be used continuously until a latitude 15 deg above the ecliptic plane has been reached. A latitude rather than an orbit inclination has been specified so that the power supply will still be within its nominal lifetime when the maximum latitude is reached. If an inclination of 15 deg had been specified, the vehicle might have to coast for as long as five or six months before coming to the desired 15 deg latitude. It is probable that the trajectories considered herein can be improved somewhat by introducing coast periods, but these would complicate the analysis, and it is believed that the maximum improvement that can be produced is less than 6%. This subject is considered further in Appendix V.

The propulsion requirements for this mission are roughly the same as those for the Mars satellite and for the Mercury probe, and the relative standing of the ion rocket and the chemical rocket is about the same. One further possibility that has been considered is the use of chemical rocket engines and ion engines in combination (Ref. 9). The out-of-the-ecliptic probe is probably the most promising mission considered here for the use of this dual-thrust mode of propulsion because it has the greatest difference between the ideal velocity requirements with low thrust and with high thrust. A typical dual-thrust trajectory would consist of an initial low-thrust spiral out to a high orbital altitude. At this point a chemical rocket engine using a storable propellant provides a small velocity decrement so that the vehicle descends back to the original 300 n mi altitude along a highly elliptical trajectory. At this point a large chemical-rocket impulse is given and the vehicle proceeds under ion propulsion beyond the Earth's sphere of influence. On emerging from the sphere of influence, the velocity would be directed somewhat above the ecliptic plane and low thrust would continue to be used to the end of the mission in a manner similar to that described for the case of the ion engine alone. A nitrogen tetroxide/hydrazine storable propellant combination with a vacuum specific impulse of 310 sec was assumed, since the insulation requirements for hydrogen-oxygen appear to be prohibitive in the presence of a power supply radiator.

The results for this mission are shown in Fig. 20 which compares the 60 kw ion rocket, the chemical rocket, and the dual-thrust system. The results of this figure tend to bear out the simplified analysis of Ref. 9 in showing that the dual-thrust mode of operation is always superior to low thrust alone when escaping from a central force field.

REFERENCES

1.  Eilenberg, S. L.:  Estimate of Ion Engine Power Efficiency.  Unpublished Hughes Research Laboratories Estimate, March 30, 1961.

2.  John, R. R., A. Mironer, H. Macomber, and J. F. Connors:  Arc-Jet Engine Performance - Experiment and Theory II.  ARS-IAS Preprint 61-101-1795, June 1961.

3.  Edelbaum, T. N.:  Propulsion Requirements for Controllable Satellites. ARS Journal, Vol. 31, No. 8, August 1961.

4.  London, H. S.:  A Study of Earth-Satellite to Moon-Satellite Transfers Using Nonchemical Propulsion Systems.  UAC Research Laboratories Report R-1383-1, May 1959.

5.  Perkins, F. M.:  Flight Mechanics of Low-Thrust Spacecraft.  Journal of the Aero/Space Sciences, Vol. 26, No. 5, May 1959.

6.  Edelbaum, T. N.:  A Comparison of Nonchemical Propulsion Systems for Round-Trip Mars Missions.  UAC Research Laboratories Report R-1383-2, October 1960.

7.  Melbourne, W. G.:  Interplanetary Trajectories and Payload Capabilities of Advanced Propulsion Vehicles.  JPL Technical Memorandum No. 312-76, January 1961.

8.  Lass, H. and C. B. Solloway:  The Motion of a Satellite Under the Influence of a Constant Normal Thrust.  JPL Technical Report No. 32-79, May 1961.

9.  Edelbaum, T. N.:  The Use of High- and Low-Thrust Propulsion in Combination for Space Missions.  AAS Preprint 61-104, August 1961.

10. Breakwell, J. V., R. W. Gillespie, and S. Ross:  Researches in Interplanetary Transfer.  ARS Journal, Vol. 31, No. 2, February 1961.

11. Battin, R. H.:  The Determination of Round-Trip Planetary Reconnaissance Trajectories.  Journal of the Aero/Space Sciences, Vol. 26, No. 9, September 1959.

12. Smolak, G. R. and R. H. Knoll:  Cryogenic Propellant Storage for Round Trips to Moon and Venus.  IAS Paper No. 60-23, January 1960.

LIST OF SYMBOLS

| | |
|---|---|
| a | Semi-major axis |
| A | Surface area |
| e | Eccentricity |
| E | Eccentric anomaly |
| F | Thrust |
| g | Gravitational acceleration at Earth's surface |
| h | Angular momentum |
| i | Orbital inclination |
| $\bar{i}, \bar{j}, \bar{k}$ | Mutually orthogonal unit vectors |
| I | Specific impulse |
| j | Energy |
| $\ell$ | Latitude, measured from the ecliptic |
| L | Angles related to ballistic interplanetary transfer |
| $L_p$ | Heat of vaporization |
| m | Mass |
| N | Number of insulation foils |
| $\bar{N}$ | Vector normal to plane of transfer orbit |
| p | Semi-latus rectum |
| q | Heat transfer rate |
| Q | Total heat transfer rate |
| r | Radius |
| t | Time |

## LIST OF SYMBOLS
### (contd.)

$T_p, T_r$     Absolute temperature of propellant and heat source, respectively

u     Offset angle of pole of small circle from celestial pole

$V_p$     Propellant volume

V     Velocity

$\Delta V$     Characteristic velocity

W     Weight

$W_i$     Insulation weight per unit area per foil

x,y,z     Cartesian coordinates

$\alpha$     Normal steering angle

$\beta$     Radial steering angle

$\gamma$     Angle in out-of-the-ecliptic mission analysis

$\delta$     Angular displacement of center of small circle from center of great circle

$\epsilon$     Emissivity and absorptivity

$\bar{\eta}$     Vector on line of nodes

$\theta$     Polar angle measured in plane of the ecliptic

$\kappa$     Angle between x-axis and line of nodes

$\lambda$     Lagrange multiplier

$\mu$     Gravitational constant of the Sun

$\nu$     True anomaly

$\xi$     Angle from Mercury's perihelion to arrival radius vector

$\rho_p$     Propellant density

LIST OF SYMBOLS
(contd.)

$\sigma$         Stefan-Boltzmann constant

$\tau$         Year of arrival at destination

$\phi$         Angle between y-axis and Mercury's perihelion

$\Phi$         Angle used in Mercury probe analysis

$\omega$         True orbital longitude of perihelion

$\Omega$         Longitude of ascending node

## Subscripts

a         Aphelion

A         Arrival

b         Burnout

e         Earth

L         Launch

m         Mercury

o         Initial or reference conditions

p         Perihelion (also, propellant in insulation weight analysis)

APPENDIX I

ASSUMPTIONS IN TRAJECTORY ANALYSES

All trajectory calculations are based on the following simplifying assumptions:

(1) Each mission is treated as a series of two-body problems.

Although a space vehicle is at all times under the simultaneous gravitational influence of a large number of celestial bodies including the planets, their moons, and the Sun, its motion may be calculated by neglecting the gravitational effects of all except one of the bodies. The position of the vehicle in space relative to the various celestial bodies determines which of the bodies is used; the appropriate body may differ during different portions of the flight. For example, during a Mars satellite mission it is necessary to successively consider the gravitational force of the Earth, the Sun, and Mars during Earth escape, interplanetary transfer, and Mars capture portions of the trajectory, respectively. The exact point at which the switch is made from one reference body to another is based upon the sphere of influence concept, which is that for any two gravitational masses there is a sphere of influence around the smaller of the two outside of which its effects may be neglected and inside of which the effects of the larger mass may be neglected. The radius of this sphere is equal to the ratio of the smaller mass to the larger mass, to the 2/5 power, times the distance between the two bodies (Ref. 4). For example, the radius of the sphere of influence of the Earth with respect to the Sun is approximately 585,000 st mi.

(2) The planets, Sun, and the Moon are all spherical in shape and homogeneous. Thus, higher harmonics in the gravitational potential fields are neglected.

(3) The space vehicles always operate at sufficiently high altitudes so that atmospheric effects can be neglected.

(4) Other perturbing forces such as radiation pressure, electromagnetic forces, etc., are negligible.

(5) The ion rocket operates at constant thrust and constant specific impulse.

(6) The vehicle's attitude is controlled so that the thrust vector is always oriented in accordance with a predetermined steering program.

(7) In the calculation of lunar satellite missions, only trajectories which are coplanar with the Moon's motion are considered. In addition, the Moon's orbit about the Earth is assumed to be circular.

(8) The Earth's orbit about the Sun is circular. Mars' heliocentric orbit was also considered to be circular and coplanar with the Earth's orbit. In the calculation of Mercury probe trajectories, however, both the eccentricity and the inclination of Mercury's orbit are taken into account.

APPENDIX II

HIGH-THRUST INTERPLANETARY PROGRAM

An iterative procedure is used to determine the ballistic trajectory which will enable a space vehicle to leave a planet at a given date $t_1$ and arrive at a second planet at a date $t_2$. By varying the trip time, $t_2 - t_1$, and the launch date, the velocity requirements for the mission during any given time period are determined as a function of launch date and trip time. The method of solution is similar to those previously reported in Refs. 10 and 11.

It is assumed that during the time period under consideration the perturbations of the planetary orbits may be neglected and the orbits can therefore be considered as perfect ellipses. It is then necessary to specify only the launch date, arrival date, the planetary orbit elements, and the astronomical constants. The computation proceeds as follows.

Having specified the launch date, $t_1$, the eccentric anomaly $E_1$ of planet 1 at the launch is determined iteratively from the equation

$$E_1 = E_{1_{NODE}} + e_1 (\sin E_1 - \sin E_{1_{NODE}}) + \frac{\sqrt{\mu}}{a_1^{3/2}} (t_1 - t_{1_{NODE}}) \qquad (6)$$

where $t_{1_{NODE}}$ and $E_{1_{NODE}}$ are respectively the date at which planet 1 crosses the line of nodes and its eccentric anomaly at this time, $e_1$ and $a_1$ are the eccentricity and semi-major axis of the orbit of planet 1, and $\mu$ is the gravitational constant of the Sun. A first guess is made by neglecting the term $e_1 (\sin E_1 - \sin E_{1_{NODE}})$; the second guess is then made by letting this term equal $e_1 (\sin E_{1_0} - \sin E_{1_{NODE}})$ where $E_{1_0}$ is the value of $E_1$ calculated from the first guess. This procedure is repeated until $E_1$ converges to within a specified tolerance. Since the eccentricities of the planetary orbits are small, the convergence is quite rapid.

The angular distance of the planet from its perihelion (true anomaly) at the launch date is then calculated from

$$\nu_1 = 2 \tan^{-1} \left( \sqrt{\frac{1 + e_1}{1 - e_1}} \tan \frac{E_1}{2} \right) \qquad (7)$$

The eccentric anomaly and true anomaly of planet 2 at the arrival date are determined in an identical manner.

Consider next the geometry of the interplanetary transfer. In the sketch below **s** represents the Sun, $P_1$ the planet of departure at the time of departure, $P_2$ the planet of arrival at the arrival date, $\Pi_1$ and $\Pi_2$ the planes of planetary motion, and $\Pi$ is the plane of the transfer orbit. The angles $L_1$ and $L_2$ are the arcs of the planetary orbits from the ascending node to the departure and arrival points respectively projected onto a reference sphere. Similarly, $L$ is the angle subtended by the transfer orbit between the departure and arrival points. The angles $L_1$ and $L_2$ are given by $L_1 = \nu_1 - \nu_{1_{NODE}}$, $L_2 = \nu_2 - \nu_{2_{NODE}}$. The angle of inclination between the planetary orbits is designated $i$. This angle is exaggerated in the sketch for the sake of clarity.
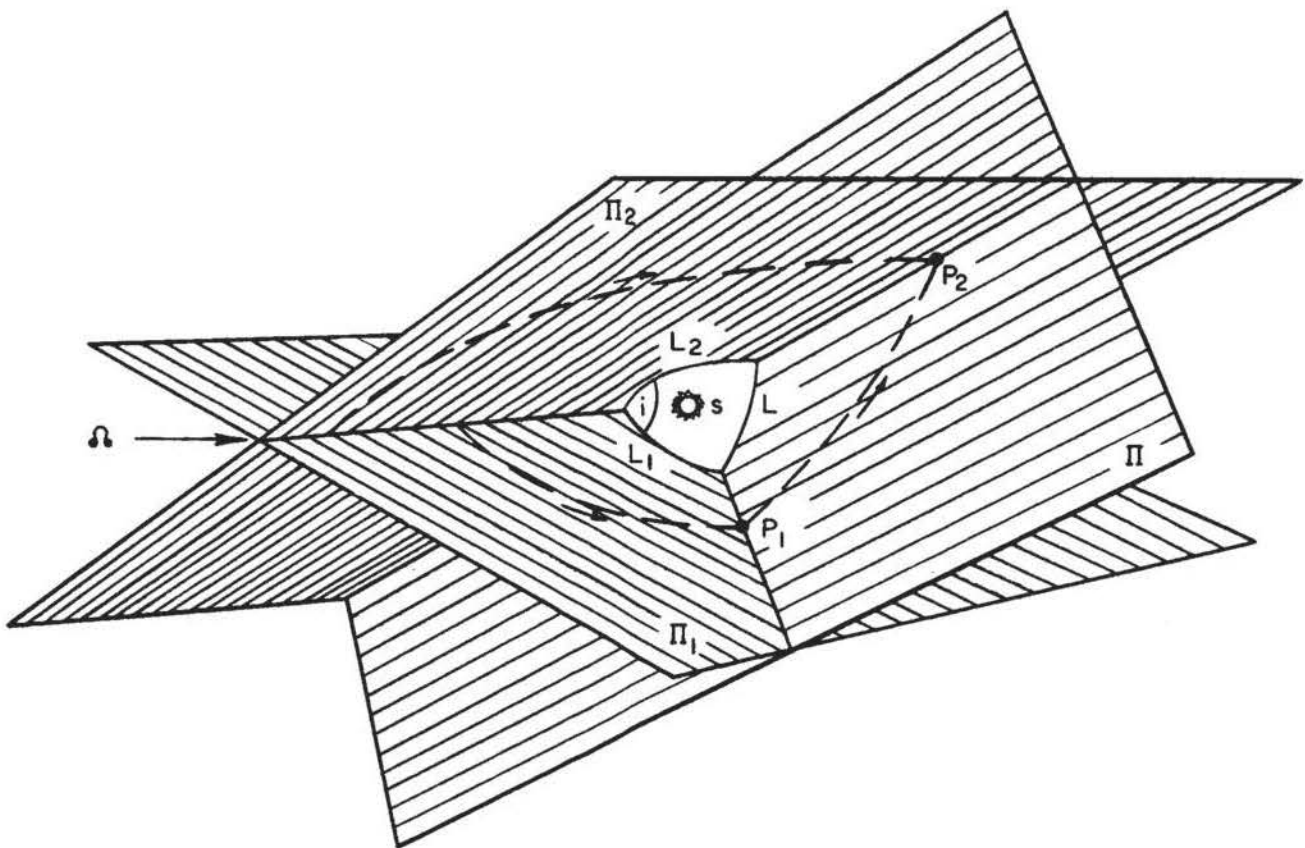


The angle of arc of the transfer trajectory $L$, is then determined from the spherical triangle:

$$\cos L = \cos L_1 \cos L_2 + \sin L_1 \sin L_2 \cos i \tag{8}$$

The above equation always has two roots; however, one corresponds to a retrograde launching and is automatically rejected in the computing program.

The launch and arrival positions are given in terms of the orbital elements of the transfer trajectory by

$$r_1 = \frac{p}{1 + e\cos\nu} \tag{9}$$

$$r_2 = \frac{p}{1 + e\cos(\nu + L)} \tag{10}$$

where $\nu$ is the true anomaly of the spacecraft on the transfer trajectory at the time of launch and $p$ is the semi-latus rectum of the transfer trajectory. Dividing these equations gives

$$\frac{r_2}{r_1} = \frac{1 + e\cos\nu}{1 + e\cos(\nu + L)} \tag{11}$$

The value of $\nu$ corresponding to the trajectory which will accomplish the transfer in the specified time is not known beforehand; it is guessed at and the above equation is then solved for the eccentricity:

$$e = \frac{\frac{r_2}{r_1} - 1}{\cos\nu - \frac{r_2}{r_1}\cos(\nu + L)} \tag{12}$$

Depending on whether $e$ is less than, equal to, or greater than one, the remainder of the calculation employs formulas for elliptic, parabolic, or hyperbolic trajectories respectively. However, the following discussion is confined to the elliptic case for the sake of brevity, the other cases being completely analogous. Thus, if $e < 1$ , the semi-major axis of the transfer trajectory is calculated from

$$a = \frac{r_1(1 + e\cos\nu)}{1 - e^2} \tag{13}$$

The eccentric anomalies on the transfer trajectory at launch and arrival are then calculated from

$$E_L = \cos^{-1}\left(\frac{1 - \frac{r_1}{a}}{e}\right) : \quad E_A = \cos^{-1}\left(\frac{1 - \frac{r_2}{a}}{e}\right) \tag{14}$$

23

Finally, the transfer time on this "guessed" trajectory is calculated from

$$\Delta t = \frac{a^{3/2}}{\mu^{1/2}} \left[ E_A - E_L - e \left( \sin E_A - \sin E_L \right) \right] \qquad (15)$$

This $\Delta t$ is compared with the desired value, $t_2 - t_1$ , and if it is not within a given tolerance, $\nu$ is incremented by a fixed amount $\Delta \nu$, the procedure is repeated, etc. until the correct value of $\nu$ is bracketed. A simple linear interpolation scheme is then used to determine the correct value of $\nu$ precisely. The initial guess for $\nu$ in the first case is made in the vicinity of 0 for transfer to an outer planet and near $\pi$ for transfer to an inner planet. Since many cases are run together, the initial guess for $\nu$ in each successive case is taken as the solution for $\nu$ of the previous case plus or minus a few degrees; thus only 2 or 3 values of $\nu$ must be tried in order to bracket the correct value.

The computing program involves numerous additional tests and "if" statements in order to resolve ambiguities in the various angles and to reject physically meaningless cases (e.g., negative $e$ or $a$ ). Nevertheless, approximately 6000 trajectories per hour can be calculated on the Philco 2000 digital computer.

After the elements of the transfer orbit have been determined, the heliocentric velocities relative to the planets at departure and arrival are calculated by vectorial subtraction of the planet's and spacecraft's velocities. Finally, these heliocentric relative velocities are translated into the required planetocentric velocities at any specified altitudes.

APPENDIX III

LOW-THRUST INTERPLANETARY PROGRAM (ORBITERS)

The heliocentric portions of the low-thrust trajectories are assumed to consist of three parts: (1) departure from the Earth's orbit using a constant thrust vector angle $\beta$, measured from the circumferential direction as shown in the sketch below; (2) a ballistic coast, and (3) powered approach into the orbit of the destination planet using a constant thrust vector angle $-\beta$.
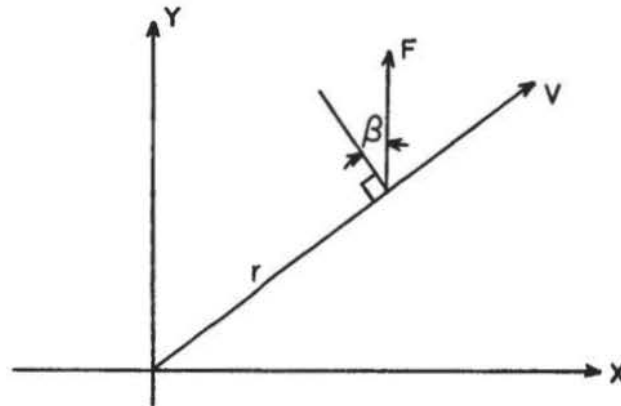


In the above sketch X & Y are the Cartesian coordinates of the space vehicle.

Studies at NASA Lewis Laboratories have shown that a constant thrust vector angle closely approximates the steering program which minimizes transfer time between coplanar circular orbits.

The equations of motion of the powered portions of the trajectory are numerically integrated in Cartesian coordinates using a Runge-Kutta starting procedure and a second-order Cowell integration method. These equations are

$$\ddot{X} + \frac{\mu X}{r^3} = \frac{F}{m} \frac{X \sin \beta - Y \cos \beta}{\sqrt{X^2 + Y^2}} \tag{16}$$

$$\ddot{Y} + \frac{\mu Y}{r^3} = \frac{F}{m} \frac{Y \sin \beta + X \cos \beta}{\sqrt{X^2 + Y^2}} \tag{17}$$

$$m = m_0 - \dot{m}t \tag{18}$$

where F is the thrust, m the instantaneous mass, and $\dot{m}$ is the propellant flow rate, assumed to be constant.

The times at which the coast is started and terminated are determined by matching instantaneous orbital parameters of the two powered phases, as follows:

A powered Earth departure trajectory is obtained by numerically integrating the equations of motion for an arbitrarily specified length of time. At each point on this trajectory the energy and angular momentum are determined and plotted against each other. Then the equations are integrated backwards starting from the orbit of the target planet, and again the instantaneous energy is plotted against the instantaneous angular momentum.

Since energy, $j$ , and angular momentum, $h$ , are constant during coasting, the intersection of the two $j-h$ curves will determine coasting period and therefore a completely matched transfer trajectory. That is, the spacecraft departs from the Earth's orbit with power on until the intersection point of the $j-h$ curve is reached, and the power is then shut off. The vehicle is then allowed to coast until it reaches the intersection point of the $j-h$ curve as determined from the backwards integration of the planetary orbit approach; at this point the thrust is turned back on and the vehicle will arrive at the destination orbit with the correct velocity. One additional step is necessary in the complete determination of the trajectory; that is, since the total powered time is not known to begin with, the mass of the spacecraft upon arrival at the orbit of the target planet must be guessed at in order to specify an initial mass for the backwards integration. With this initial guess specified, the integrations are carried out, the required burning time determined, and the final mass compared with the initial guess. If it is not sufficiently close, the integrations can be run again with successive new guesses for the final mass until a close enough convergence is obtained. Alternately, the backwards integration can be run with several different values of the final mass and the correct value subsequently determined by interpolation of the results. In either case, with high specific impulse electrical propulsion systems the propellant consumed during the interplanetary phase is usually small enough so that fairly good guesses can be made and little trial and error is necessary.

In this manner a trajectory is determined for each selected value of the steering angle $\beta$, each different $\beta$ resulting in a different powered time and coasting time. A curve of propellant consumption vs total trip time is thereby arrived at; generally as $\beta$ is increased from 0 deg the powered time and therefore propellant consumed increases, while the coasting time decreases. At some value of $\beta$, usually around 60 or 70 deg, the total time will be a minimum, and will then increase again approaching infinity as $\beta$ approaches 90 deg. This is due to the fact that an orbit-to-orbit transfer is impossible with $\beta = 90$ deg since the angular momentum does not change.

Thus by changing $\beta$ a curve of payload vs trip time is determined for a given value of the specific impulse. Repeating the procedure for various specific impulses, an envelope may then be drawn by picking the specific impulse for which the payload is maximum for each given trip time.

APPENDIX IV

LOW-THRUST MERCURY PROBE PROGRAM

Object

The program described in this Appendix was developed to permit rapid calcu-
lation of one-way, low-thrust Mercury probe missions.  The analysis yields a
three-dimensional solution and also accounts for the eccentricity of Mercury's
orbit.

Assumptions

1.  Initial conditions for the probe correspond to the position and velocity
of the Earth.

2.  The steering angle is held constant over the entire powered phase of
the trajectory.

3.  Since Mercury's inclination to the ecliptic is small (7 deg), the "out-
of-the-ecliptic" components of thrust, acceleration, etc. may be uncoupled from
the "ecliptic" components in integrating the equations of motion.

4.  The trajectory consists of an initial low-thrust phase followed by a
ballistic transfer to the target planet.

Logic

1.  Select an arrival position

   One arrival position corresponds to four or five possible arrival
   dates in the year 1968 (period, $T_M$ = 88 days; 365/88 $\approx$ 4.16)

2.  Select specific impulse $I$ , thrust $F$ , initial mass $m_0$ , and steering
   angles

   a. $\beta$ = radial steering angle

   b. $\alpha$ = normal (to ecliptic) steering angle

3.  Using polar coordinates $r$ and $\theta$ , integrate the equations of motion in
   two dimensions.  Angular position at launch is not specified.

27

4. At each step of integration determine the transfer ellipse which would result if powered flight were terminated at that point.

   a. When the perihelion $r_p$, of the instantaneous transfer ellipse equals the arrival radius vector $r_A$, a "hit" becomes possible (Mercury is an interior planet).

   b. For all subsequent steps in the integration, "hit" transfer trajectories are possible.

5. A "hit" only occurs if both launch and arrival positions of the probe and terminal planets match up.

6. For each possible transfer ($r_p \le r_A$) determine the required launch position angle $\nu_{Lp}$.

   a. The total transfer angle is the sum of the powered and ballistic transfer angles.

   b. The arrival position angle is known since the arrival position itself was selected at the beginning.

7. The actual position angle of the Earth $\nu_{Le}$ can be determined from the arrival date, total trip time, and the known position of the Earth at some reference date.

8. When $\nu_{Le} = \nu_{Lp}$ (within some tolerance) a two-dimensional hit occurs.

9. In general $\nu_{Le} \neq \nu_{Lp}$ and no solution exists for that particular powered time.

   a. When $\nu_{Le} \neq \nu_{Lp}$ return and integrate forward another step.

   b. Continue until a solution is found.

10. At each instant of time eight possible solutions must be considered.

   a. There are four possible arrival dates.

   b. Given a position and velocity vector, there exist two transfer ellipses to a fixed terminal.

11. For each two-dimensional solution try to match the probe elevation (altitude above ecliptic) with Mercury's elevation at the target point.

a.  The equation of motion normal to the ecliptic (Z direction) has been uncoupled.

b.  This equation is integrable so that for any normal steering angle $\alpha$, the elevation at burn-out is known.

c.  The characteristics (including inclination) of the transfer ellipse are known from conditions at burn-out.

d.  The total elevation $Z_p$, of the probe at the arrival point can therefore be calculated.

e.  Changing the steering angle affects $Z_p$ because the inclination of the transfer ellipse is changed.

f.  If the probe passes through a node during the ballistic phase, increasing $\alpha$ (more positive) will decrease $Z_p$ (more negative).

g.  If the arrival point happens to fall at or near a node (of the transfer ellipse), no three-dimensional solution may exist since changing the inclination of the orbit has little effect on the elevation of points near the node.

h.  Only solutions involving small $\alpha$'s are acceptable.

12. Continue the integration until the aphelion radius $r_a$ of the transfer orbit is less than $r_A$.

13. Best solutions (lowest $\Delta V$) should correspond to arrival near Mercury's aphelion but since the time period is limited to launches in 1968, only a limited number of solutions will exist near this arrival point.

14. In order to plot $\Delta V$ vs launch date, many trajectories must be run for a complete range of arrival points in Mercury's orbit and for a range of radial steering angles (normal steering angle, $\alpha$ has a negligible effect on $\Delta V$ as long as $\alpha$ is small).

15. The numerous solutions can be grouped according to trip times and for each group a plot of $\Delta V$ vs launch date obtained.

Analysis

The equations of motion are:

$$\ddot{r} - r\dot{\theta}^2 + \frac{\mu}{r^2} - \frac{F\cos\beta}{m_0 - \dot{m}t} = 0 \tag{16}$$

$$\frac{1}{r} \frac{d}{dt} \left( r^2 \dot{\theta} \right) - \frac{F \sin \beta}{m_0 - \dot{m}t} = 0 \qquad (17)$$

$$\ddot{Z} - \frac{F \sin \alpha}{m_0 - \dot{m}t} = 0 \qquad (18)$$

where in Eq. (18) it has been assumed that the elevation is small so that the $Z$ - component of gravitational force, $\mu Z / r^3$, can be neglected with respect to the normal component of thrust.

$$\dot{m} = \frac{F}{I} \qquad (19)$$

The numerical integration of Eq.'s (16) and (17) proceeds from initial conditions:

$$t = 0, \quad \theta = 0, \quad r = r_e, \quad \dot{\theta} = \dot{\theta}_e, \quad \dot{r} = 0 \qquad (20)$$

where

$$\dot{\theta}_e = \sqrt{\frac{\mu}{r_e^3}} \qquad (21)$$

At each instant of time calculate the elements of the transfer ellipse:

$$\frac{1}{a} = \frac{2}{r} - \frac{\dot{r}^2 + (r\dot{\theta})^2}{\mu} \qquad (22)$$

$$e = \sqrt{\frac{r^2 \dot{r}^2}{\mu a} + \left( 1 - \frac{r}{a} \right)^2} \qquad (23)$$

$$r_p = a(1-e) \qquad (24)$$

When $r_p \leq r_a$ a two-dimensional hit may be possible because the transfer ellipse can pass through the destination point. Since the launch point has not been specified (except that $r_L = r_e$) any path for which $r_p \leq r_A$ can pass through the arrival point. In fact two ellipses exist for each burnout time. (The time $t$ for which a transfer ellipse is determined is called the burnout time.)

The elements of the ellipse are completely determined by the position and velocity at burnout and the arrival position.

30

$$\cos E_b = \frac{1}{e}\left(1 - \frac{r_b}{a}\right) \tag{25}$$

$$\sin E_b = \frac{r_b \, \dot{r}_b}{e\sqrt{\mu a}} \tag{26}$$

With $E_b$ thus defined $\nu_b$ is obtained from:

$$\cos \nu_b = \frac{a}{r_b}\left(\cos E_b - e\right) \tag{27}$$

The quadrant of $\nu_b$ is determined by the following rules.

| Quadrant of $E_b$ | Sign of $\cos \nu_b$ | Quadrant of $\nu_b$ |
|---|---|---|
| 1 | >0 | 1 |
|   | <0 | 2 |
| 2 | >0 | Impossible |
|   | <0 | 2 |
| 3 | >0 | Impossible |
|   | <0 | 3 |
| 4 | >0 | 4 |
|   | <0 | 3 |

Similarly,

$$\cos E_A = \frac{1}{e}\left(1 - \frac{r_A}{a}\right) \tag{28}$$

$$\cos \nu_A = \frac{a}{r_A}\left(\cos E_A - e\right) \tag{29}$$

31

Since neither $E_A$ nor $\nu_A$ is uniquely defined by these equations it is apparent that more than one ellipse can be drawn through the arrival point.

| Sign of $\cos E_A$ | Quadrant of $E_A$ | Sign of $\cos \nu_A$ | Quadrant of $\nu_A$ |
|---|---|---|---|
| 0 | 1 | >0 | 1 |
| | | <0 | 2 |
| | 4 | >0 | 4 |
| | | <0 | 3 |
| 0 | 2 | >0 | Impossible |
| | | <0 | 2 |
| | 3 | >0 | Impossible |
| | | <0 | 3 |
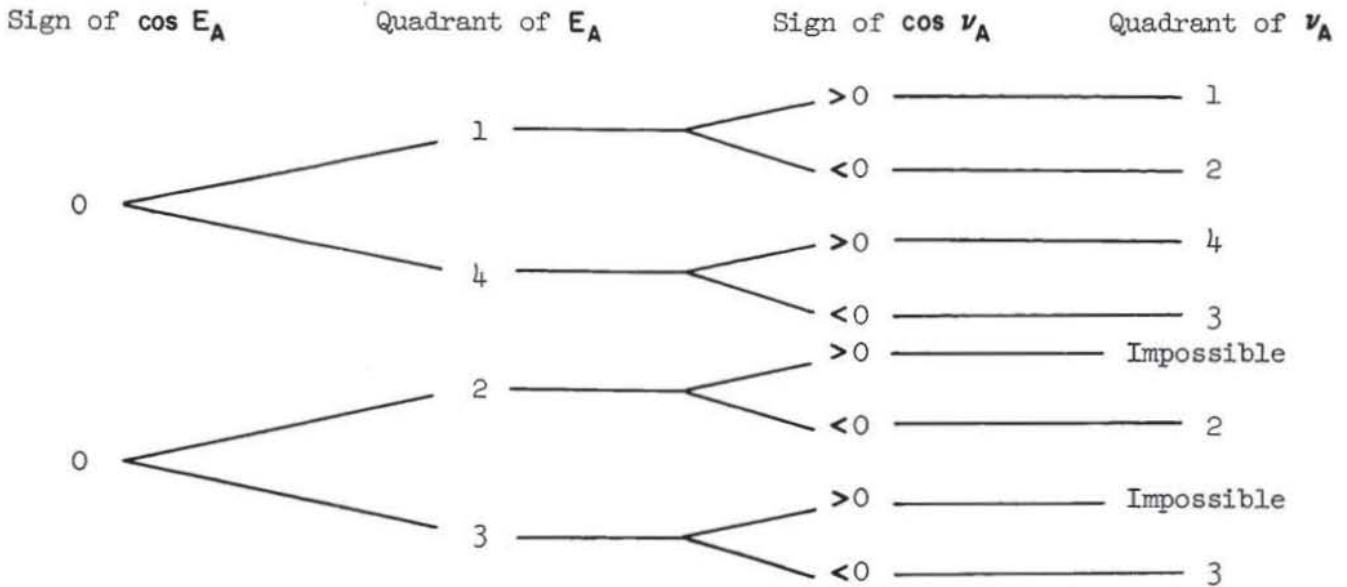
Two values of $E_A$ and $\nu_A$ must be considered from this point on. Let $E_{Aj}$ and $\nu_{Aj}$ represent these solutions and let $j = 1, 2$.

Referring to Fig. 21 the angular position of the probe at launch is calculated as follows:

$$\nu_{Lpj} = \nu_b - \theta - \phi - \xi - \nu_{Aj} + \pi \tag{30}$$

and the total trip time, $t_j$, is the sum of the powered time, $t_b$, and the ballistic time, $t_{uj}$, where

$$t_{uj} = \sqrt{\frac{a^3}{\mu}} \left\{ e \left( \sin E_b - \sin E_{Aj} \right) + \left( E_{Aj} - E_b \right) \right\} \tag{31}$$

and

$$t_{tj} = t_b + t_{uj} \tag{32}$$

Since the position of the probe at launch must coincide with the Earth's position on that date, $\nu_{Lpj}$ must be equal to some angular position $\nu_{Lej}$ in order for a hit to occur.

$$\nu_{Lej} = \nu_{eo} + \dot{\theta}_e \left( t_{Ak} - t_{tj} \right) \tag{33}$$

where $k = 1, 2, 3, 4$ (for Mercury) corresponds to each of the four arrival dates for a given arrival position of Mercury.

If the arrival times, $t_{Ak}$, are measured from some fixed reference date $t_o = 0$ the time represented by the bracket in Eq. (33) is the launch date. The reference angle $\nu_{eo}$ is the angular position of the Earth (measured from perihelion) on the reference date.

In general, $\nu_{Lej} \neq \nu_{Lpj}$ and the launch positions of Earth and probe are not coincident. This means that of eight possible solutions (summing over $j$ and $k$), none are two-dimensional hits for the particular burnout time under consideration. Consequently the integration of the equations of motion is carried out for another increment of time and the procedure repeated. Although no solutions will occur for most time increments, the machine program must be capable of handling eight separate cases, each alone or any number of which may be solutions.

When a two-dimensional hit occurs, the normal steering angle, $\alpha$, must be adjusted so that $Z_p = Z_a$. The equation of motion is Eq. (18) which can be integrated to yield

$$\dot{Z}_b = \frac{-F \sin \alpha}{\dot{m}} \ln \left\{ 1 - \frac{\dot{m}}{m_o} t_b \right\} \tag{34}$$

and

$$Z_b = \frac{m_o F \sin \alpha}{\dot{m}^2} \left\{ \frac{\dot{m}}{m_o} t_b + \left( 1 - \frac{\dot{m}}{m_o} t_b \right) \ln \left[ 1 - \frac{\dot{m}}{m_o} t_b \right] \right\} \tag{35}$$

With conditions at burnout known, it remains to determine the effect of inclination of the transfer orbit on the elevation of the probe. Referring to Fig. 22, two vectors, $\bar{r}_b$ and $\bar{V}_b$, are defined in an orthogonal coordinate system with the origin at the Sun and the $y$ axis in the direction of the Earth's aphelion. Define the angles:

$$\zeta = \frac{\pi}{2} + \kappa - (\phi + \xi) \tag{36}$$

$$\delta_j = \nu_b + \frac{3\pi}{2} - \nu_{aj} - (\phi + \xi)$$ (37)

$$\Phi_j = \delta_j - \frac{3\pi}{2}$$ (38)

Then the **x** and **y** components of $\bar{r}_b$ and $\bar{V}_b$ are:

$$X_{bj} = -r_b \sin \Phi_j$$ (39)

$$Y_{bj} = r_b \cos \Phi_j$$ (40)

$$\dot{X}_{bj} = -r_b \dot{\theta}_b \cos \Phi_j - \dot{r}_b \sin \Phi_j$$ (41)

$$\dot{Y}_{bj} = -r_b \dot{\theta}_b \sin \Phi_j + \dot{r}_b \cos \Phi_j$$ (42)

Define a vector $\bar{N}$ normal to the plane of the transfer orbit.

$$\bar{N} = \bar{V}_b \times \bar{r}_b = N_x \bar{i} + N_y \bar{j} + N_z \bar{k}$$ (43)

where

$$N_x = \dot{Y}_b Z_b - \dot{Z}_b Y_b$$ (44)

$$N_y = \dot{Z}_b X_b - \dot{X}_b Z_b$$ (45)

$$N_z = \dot{X}_b Y_b - \dot{Y}_b X_b$$ (46)

The line of nodes is then determined since it lies in both the plane of the transfer orbit and the ecliptic. If $\bar{\eta}$ represents a vector on the line of nodes:

$$\bar{\eta} = \bar{N} \times \bar{k} = N_y \bar{i} - N_x \bar{j} \tag{47}$$

Referring again to Fig. 22, the angle $\kappa$, between the line of nodes and the **x** axis, is now determinate.

$$\cos \kappa = \frac{-\bar{\eta} \cdot \bar{i}}{|\bar{\eta}|} = \frac{-N_y}{\sqrt{N_x^2 + N_y^2}} \tag{48}$$

$$\sin \kappa = \frac{|\bar{\eta} \times \bar{i}|}{|\bar{\eta}|} = \frac{-N_x}{\sqrt{N_x^2 + N_y^2}} \tag{49}$$

The inclination of the transfer orbit is obtained as follows.

$$\cos i = \frac{\bar{N} \cdot \bar{k}}{|\bar{N}|} = \frac{N_z}{\sqrt{N_x^2 + N_y^2 + N_z^2}} \tag{50}$$

$$\tan i = \frac{\sqrt{N_x^2 + N_y^2}}{N_z} \tag{51}$$

With these parameters known the elevation of the probe is:

$$Z_p = \frac{r_A \tan i \sin \zeta}{\sqrt{1 + \tan^2 i \sin^2 \zeta}} \tag{52}$$

or

$$Z_p = \frac{-r_A \tan i \left( N_y \cos(\phi + \xi) + N_x \sin(\phi + \xi) \right)}{\sqrt{N_x^2 + N_y^2 + \tan^2 i \left( N_y \cos(\phi + \xi) + N_x \sin(\phi + \xi) \right)^2}} \tag{53}$$

By trial and error, $Z_p$ can be adjusted to equal $Z_A$ by changing $\alpha$. The procedure is first to determine whether a positive increase in $\alpha$ causes a positive increase in $Z_p$. If one of the nodes of the transfer orbit lies between the burnout and arrival points this will not be true. Also, if the arrival point happens to fall near one of the nodes, $Z_p$ will be relatively insensitive to changes in $\alpha$ and in some instances a solution may not be possible. Since one of the assumptions made in the analysis is that the normal component of thrust is small, only small values of $\alpha$ are acceptable as solutions.

After each three-dimensional solution is either obtained or the case discarded as impossible, the two-dimensional integration is continued and the entire procedure repeated for each solution.  The case may be terminated after some preset maximum burning time or else allowed to continue until the aphelion radius of the transfer orbit

$$r_{ap} = a(1+e) \tag{54}$$

is less than $r_A$.

After each solution the ideal velocity, $\Delta V$, is calculated from

$$\Delta V = gI \ln \left\{ \frac{m_0}{m_0 - \dot{m}_{tb}} \right\} \tag{55}$$

### Input Data

It is convenient to allow the machine to calculate the input as much as is practicable.  The following equations can be used to determine the characteristics of the arrival points with only Mercury's true anomaly, $\nu_{Am}$, and the time period, $\tau$ , known.

$$\xi = \pi - \nu_{Am} \tag{56}$$

$$p_m = a_m (1 - \epsilon_m^2) \tag{57}$$

$$r_A = \frac{p_m}{1 + \epsilon_m \cos \nu_{am}} \tag{58}$$

$$\omega_m = \kappa_m - \Omega_m + (\tau - 1961)(\dot{\Omega} + \dot{\kappa}) \tag{59}$$

where $\dot{\Omega}$ and $\dot{\kappa}$ are corrections for the mean equinox of the arrival period.

At a reference date designated by the subscript O, Mercury's position is known.

$$r_0 = \frac{p_m}{1 + e_m \cos \nu_{om}} \tag{60}$$

$$\cos E_{om} = \frac{r_o}{a_m} \cos \nu_{om} + e_m \tag{61}$$

$$\cos E_{Am} = \frac{r_A}{a_m} \cos \nu_{Am} + \epsilon_m \tag{62}$$

The time of arrival is:

$$t_{Ak} = (k-1)T_m + \sqrt{\frac{a_m^3}{\mu}} \left\{ \epsilon_m (\sin E_{Am} + \sin E_{om}) - (E_{om} + E_{Am}) \right\} \tag{63}$$

where $k = 1, 2, 3, 4$ and $0 \leq t_{Ak} \leq T_e$ \hfill (64)

Mercury's elevation is

$$Z_A = \frac{r_A \tan i_m \sin(\xi - \omega_m)}{\sqrt{1 + \tan^2 i_m \sin^2(\xi - \omega_m)}} \tag{65}$$

APPENDIX V


OUT-OF-THE-ECLIPTIC MISSION


This appendix presents a derivation of the method used to calculate low-thrust out-of-the-ecliptic trajectories. This method provides a near-optimum closed-form analytic solution for the trajectory and the propulsion requirements that are valid for celestial latitudes up to approximately 15 deg. The basis of the method is the fact that a vehicle describing a circular orbit under the influence of a constant acceleration normal to the orbit will describe a small circle on the surface of an imaginary sphere (Ref. 8). The geometry of this small circle is illustrated in the accompanying sketch.
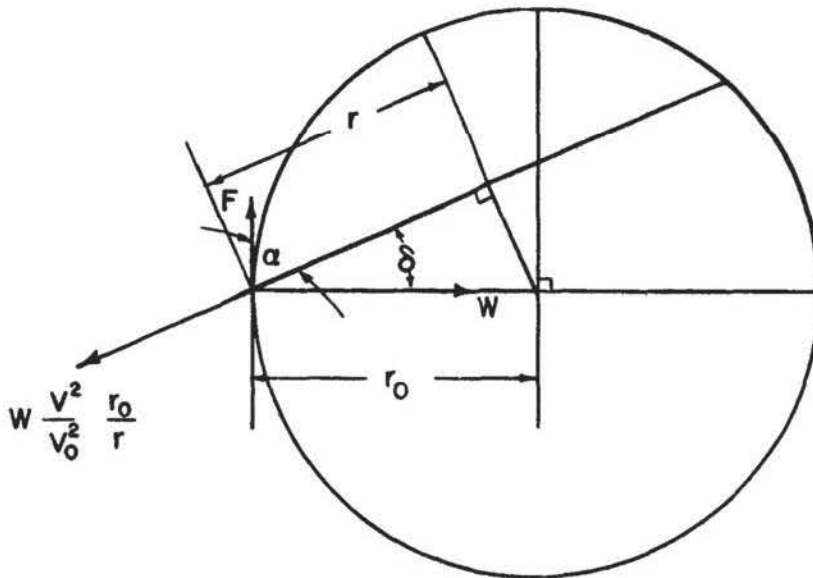


The plane of the small circle of radius $r$ makes an angle $\delta$ with the plane of the great circle whose radius is $r_0$. In order for the spacecraft to move along this small circle it is necessary for the forces shown in the figure to balance each other. By proper adjustment of the thrust angle $\alpha$, it is always possible to find an angle $\delta$ for which the vehicle will move along a small circle under the action of a constant thrust acceleration. Equating the forces along and normal to the plane of the small circle yields the following equations.

$$F \cos \alpha + W \cos \delta = \frac{W}{\cos \delta} \frac{V^2}{V_0^2} \tag{66}$$

$$W \sin \delta = F \sin \alpha \tag{67}$$

It is assumed that the velocity on the small circle is equal to the velocity of a circular orbit along a great circle so that no velocity corrections need be made. Equations (66) and (67) may then be solved to yield:

$$\alpha = \frac{\pi}{2} - \delta \tag{68}$$

$$\frac{F}{W} = \tan \delta \tag{69}$$

For the low-thrust systems under consideration, the thrust-weight ratio will always be small so that second order terms may be neglected. This assumption will introduce an error of less than 1% for latitudes up to about 18 deg, and Eq. (69) becomes:

$$\frac{F}{W} \approx \delta \tag{70}$$

The equations for celestial latitude and orbital inclination can now be developed under the assumption that the inclination and latitude are small and the fact that the vehicle moves in a small circle. Consider the small circles shown in the sketch, whose pole is displaced by the small angle u from the celestial pole.
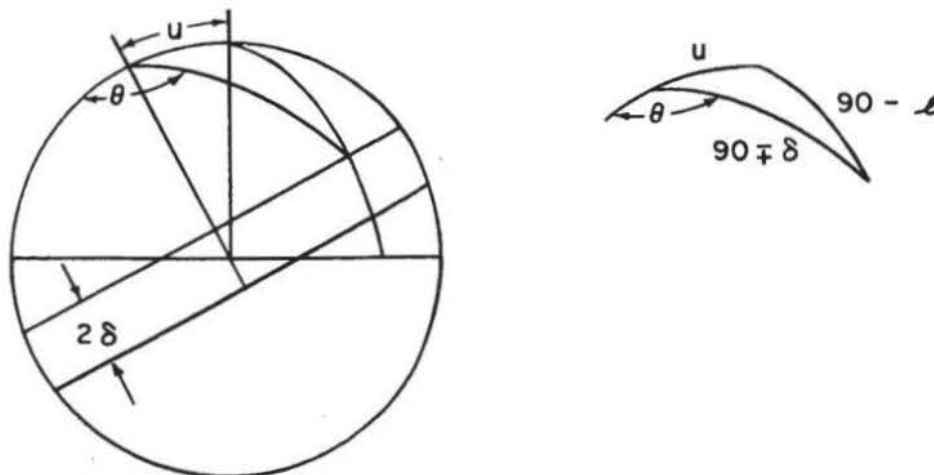
The use of spherical trigonometry for the spherical triangle shown above on the right yields

$$\sin \mathcal{L} = \pm \cos u \sin \delta - \sin u \cos \delta \cos \theta \qquad (71)$$

Eliminating second order items in $\mathcal{L}$, $u$, and $\delta$ yields Eq. (72) where the plus sign is used if the thrust is directed upward and the minus sign is used if it is directed downward.

$$\mathcal{L} = \pm \delta - u \cos \theta \qquad (72)$$

The values of the inclination $i_1$, and of $u_2$ are next to be derived for a vehicle starting from an inclination and latitude of zero, and reversing its thrust direction after moving through a central angle of $\theta_1$. The following sketches show the geometry of the problem as viewed from the celestial pole.
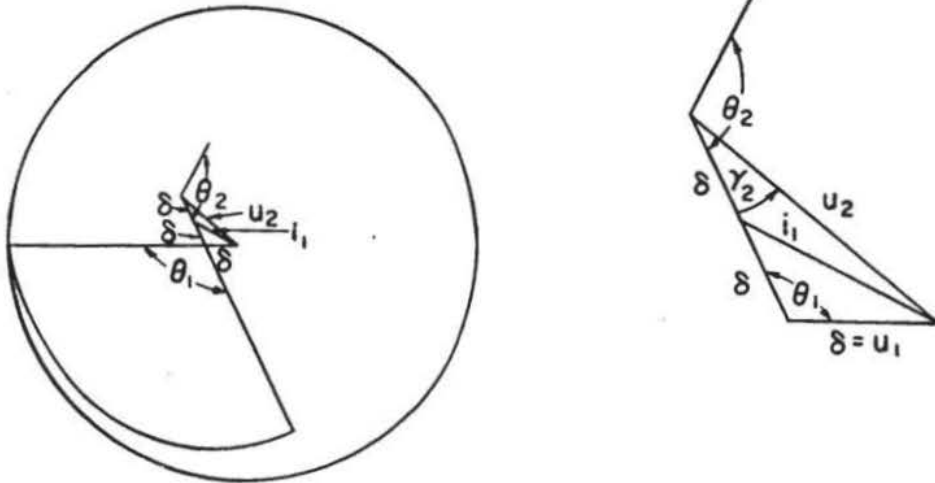


The value of $u$ for the first phase is $\delta$. The value of $i_1$, and the value of $u$ when the thrust is reversed ($u_2$) may be found from the right hand sketch. As all arc lengths are assumed small, plane trigonometry may be used.

$$i_1 = \sqrt{\delta^2 + \delta^2 - 2\delta^2 \cos\theta_1} \;\; = 2\delta \sin\frac{\theta_1}{2} \tag{73}$$

$$u_2 = \sqrt{\delta^2 + 4\delta^2 - 4\delta^2 \cos\theta_1} \;\; = \delta\sqrt{5 - 4\cos\theta_1} \tag{74}$$

The value of $\ell$ after the thrust is reversed may be found by evaluating the angle $\gamma_2$ and making use of Eq. (72).

$$\sin\gamma_2 = \delta\frac{\sin\theta_1}{u_2} \;\; = \frac{\sin\theta_1}{\sqrt{5 - 4\cos\theta_1}} \tag{75}$$

$$\cos\gamma_2 = \frac{\sqrt{5 - 4\cos\theta_1 - 1 + \cos^2\theta_1}}{\sqrt{5 - 4\cos\theta_1}} \;\; = \frac{2 - \cos\theta_1}{\sqrt{5 - 4\cos\theta_1}} \tag{76}$$

$$\ell = -\delta - u_2\cos(\theta_2 + 180° - \gamma_2) \tag{77}$$

let $\theta = \theta_1 + \theta_2$

$$\ell = -\delta + u_2\cos(\theta - \theta_1 - \gamma_2) \tag{78}$$

Some trigonometric manipulation yields the following final equation.

$$\frac{\ell}{\delta} = -1 + (2\cos\theta_1 - 1)\cos\theta + 2\sin\theta_1\sin\theta \tag{79}$$

This equation is next differentiated to find the optimum value of $\theta_1$, the point where thrust direction should be reversed 180 deg.

$$\frac{\partial\frac{\ell}{\delta}}{\partial\theta_1} = 0 = -2\sin\theta_1\cos\theta + 2\cos\theta_1\sin\theta \tag{80}$$

41

$$\tan \theta_1 = \tan \theta \qquad (81)$$

Investigation has shown that the proper quadrants for $\theta_1$, and the maximum attainable values of $\ell$ are as follows:

for $0° \leq \theta_1 \leq 180°$

$$\theta_{1_{opt}} = \theta \qquad (82)$$

$$\ell = \frac{F}{W} (1 - \cos \theta) \qquad (83)$$

for $180° \leq \theta_1 \leq 360°$

$$\theta_{1_{opt}} = \theta - 180° \qquad (84)$$

$$\ell = \frac{F}{W} (3 + \cos \theta) \qquad (85)$$

If there is an initial orbital inclination at $\theta = 0$, as is the case when dual thrust is used, this inclination will produce a periodic change in latitude which may be added linearly to Eqs. (83) and (85) within the validity of the linear approximation.

$$\ell = i_0 \sin \theta \qquad (86)$$

The above derivation results in a simple approximation to the motion of a vehicle in a central force field under the influence of a normal force. It remains to be shown how much improvement may be expected if this trajectory were optimized. The minimum-fuel maneuvers for changing inclination are known for the cases where the thrust-weight ratio is very large or infinitesimally small (Ref. 3). In both these limiting cases it is desirable to enlarge the orbit and then shrink it back to the original size while changing inclination. The decrease in required characteristic velocity due to this enlarging and shrinking of the orbit is only 0.7% for infinitesimal thrust and only 0.6% for impulsive thrust for a 15 deg inclination. The calculated maneuver, which lies in an intermediate thrust range, is apparently near-optimum.

A larger improvement in the assumed trajectory might be produced by intro-ducing coast periods. Calculations for infinitesimal thrust have shown that, if

engine efficiency is constant, a 6% larger change in inclination may be produced for a given time and given fuel consumption if optimum coast periods are used. Since the ion engines in the present problem are used in a region where efficiency is not constant, but decreases rapidly as specific impulse is reduced, the performance improvements due to introducing coast periods are probably much smaller than 6% and have been neglected.

## APPENDIX VI

### INSULATION WEIGHT

If cryogenic propellants are to be transported on interplanetary trips or during the low-thrust escape phase of some extra-terrestrial mission, an adequate thermal protection system must be provided to prevent excessive propellant boil-off. The purpose of this analysis is to design a reflecting foil insulation system which minimizes propellant boil-off for a given insulation weight.

### Assumptions

1. The vehicle arrangement is as shown in Fig. 23.

2. The propellant tanks are cylindrical.

3. Constant-temperature bodies (520 R) representing the reactor, power supply, payload, etc. are placed at each end.

4. Since solar heat flux is almost always the greatest source of radiation, it is assumed that one end of the vehicle is continuously pointed toward the Sun.

5. The heat rejection radiator extends radially outward from the tank walls and lies in a single plane.

6. The insulation consists of reflecting foils which are applied in thermally isolated layers over each surface.

7. The only source of conduction is through a simple support structure at each tank end.

8. The tanks are assumed to be full.

9. The tank walls represent an additional reflective foil.

10. Propellant temperatures are constant and all heat transferred to the propellants is accounted for by the resultant vaporization.

ANALYSIS

The sources of heat flux may be grouped into two categories (1) those which originate within the vehicle, or internal sources, and (2) external sources of radiation, such as the Sun and planets.

Within the framework of the assumption, heat transfer to the propellants may occur by three internal routes. Radiation from the power supply heat rejector is the major path since the radiator is in close proximity to the tanks and may attain a surface temperature of almost 700 F. In addition, conduction and radiation through the tank ends comprise other internal heat paths.

The largest source of heat flux in space, namely the Sun, is not of major concern since the solar radiation is never directly incident on the tank surfaces. The constant temperature body at one end of the vehicle is assumed to reach an equilibrium temperature of 520 R which it would attain under constant solar heating at Earth's distance from the Sun.

Therefore the only external heat source is the Earth. Planetary heat flux consists of emission (based on the temperature of the Earth-atmosphere system), and albedo reflection of the solar flux. These external sources are of importance only when the vehicle is close to the Earth, for example during the initial phase of a low-thrust escape.

With the vehicle components arranged as in Fig. 23, five different surfaces are exposed to heat transfer from various combinations of the above internal and external sources. Each tank end is treated as a separate surface, as are the cylindrical portions of the $O_2$ and $H_2$ tanks. The interface between tanks is the fifth surface.

The remainder of the analysis is concerned with covering each of the five surfaces with a sufficient number of foils to prevent excessive propellant vaporization. It is advantageous to optimize the distribution of foils on the various surfaces so as to achieve the most effective protection with a minimum expenditure of weight.

The rate of heat transfer to the propellant through the cylindrical wall and insulation is given by (Ref. 12):

$$\left(\frac{q}{A}\right) = \frac{Q - \epsilon \sigma T_p^4}{N(2-\epsilon)+1} \tag{87}$$

where $Q$ is the total incident heat flux rate, $N$ is the number of foils on the surface, and $T_p$ is the propellant temperature. Similarly the rate of heat

45

transfer through each end is:

$$\left(\frac{q}{A}\right) = \frac{\sigma \epsilon (T_r^4 - T_\rho^4)}{(2-\epsilon)(N+1)} \tag{88}$$

where $T_r$ is the temperature of a heat source. The resultant heat transfer rate to either propellant is then found to be:

$$q_{TOTAL} = \left(\frac{q}{A}\right)_1 A_{CYLINDER} + \left(\left(\frac{q}{A}\right)_2 + \left(\frac{q}{A}\right)_3\right) A_{END} + q_4 \tag{89}$$

$$\underbrace{CYLINDER \qquad \underset{END}{TANK} \qquad \underset{INTERFACE}{TANK}}_{RADIATION} \qquad \underbrace{\qquad}_{CONDUCTION}$$

The rate of propellant vaporization expressed as a percentage of the total initial propellant mass can be obtained from

$$\frac{\dot{m}}{m_0} = \frac{2400}{L_P V_P \rho_P} q_{TOTAL} \sim \frac{\%}{DAY} \tag{90}$$

and the weight of the insulation is

$$W_i = w_i \sum_{n=1}^{5} N_n A_n \tag{91}$$

The optimization procedure is concerned with determining the foil distribution, represented by $N_n$, which will minimize $\dot{m}$ for a fixed weight, $W_i$. Using functional notation, this is done in the following way.

$$W_i = W_i (N_n) \tag{92}$$

$$q_T = q_T(N_n) \tag{93}$$

$$\frac{\dot{m}}{m_0} = \frac{\dot{m}}{m_0} (q_T) \tag{94}$$

$$\frac{\partial \frac{\dot{m}}{m_0}}{\partial N_n} + \lambda \frac{\partial W_i}{\partial N_n} = 0 \tag{95}$$

where $\lambda$ is a Lagrange multiplier.

The resulting foil distribution is then

$$N_{n_{OPT}} = N_n \left( \epsilon, T_r, T_p, q_T, \ldots \right) \tag{96}$$

and

$$\left( \frac{\dot{m}}{m_0} \right)_{MIN} = \frac{\dot{m}}{m_0} \left( N_{n_{OPT}} \right) \tag{97}$$

In the analysis it was required that the $O_2$ vaporization rate equal the $H_2$ vaporization rate since for a fixed mixture ratio neither propellant can serve its purpose at the destination unless an equivalent percentage of the other is also left unvaporized.

## PROGRAM

Provision was made in the machine program to design a thermal protection system for any size vehicle on an interplanetary, escape, or 24-hr satellite mission. For the escape maneuver the angle between the vehicle orbit plane and the vehicle-Sun line may be arbitrarily chosen between zero and 90 deg. In general this angle should be zero since this allows the vehicle to pass through the Earth's shadow on each revolution, eliminating planetary reflection as a heat source during this "eclipse."

Input items include the total propellant mass, thrust-weight ratio, tank diameter, inclination of the escape orbit plane and interplanetary trip time (only for interplanetary missions). The results are propellant vaporization and insulation weight as a function of an arbitrary system parameter which is chosen to be the number of foils, $N_I$, on the interface between tanks. For each input value of $N_I$ the program optimizes the foil distribution and calculates the weight of vaporized propellant and the total insulation system weight.

## TABLE I

### Spacecraft Weight Assumptions (lb)

|  | Ion Engine | Arc-Jet Engine | Chemical Rocket |
|---|---|---|---|
| Gross | 8500 | 8500 | 8500 |
| Structure | 280 | 280 | 280 |
| Tankage | 0.08 x propellant wt. | 0.03 x propellant tank area (sq ft) | 0.03 x propellant tank area |
| Insulation | ---- | 0.01 x propellant tank area | optimized |
| Residual & Reserve Propellant | 0.02 x propellant wt. | 0.02 x propellant wt. | 0.02 x propellant wt. |
| Engine | 100 lb (30 kw)<br>200 lb (60 kw) | 100 lb (30 kw)<br>200 lb (60 kw) | 270 |
| Power Supply | 2000 lb (30 kw)<br>3000 lb (60 kw) | 2000 lb (30 kw)<br>3000 lb (60 kw) | --- |

## TABLE II

### Typical Weight Breakdowns (lb)

| Engine | Ion | Arc-Jet | Chemical | Chemical | Chemical |
|---|---|---|---|---|---|
| Mission | 24-hr | 24-hr | 24-hr | Lunar | Mars |
| Specific Impulse, sec | 4000 | 1075 | 420 | 420 | 420 |
| Time, days | 137 | 77 | 0.46 | 3 | 259 |
| Gross Weight | 8500 | 8500 | 8500 | 8500 | 8500 |
| Structure Weight | 280 | 280 | 280 | 280 | 280 |
| Tankage & Insulation | 93 | 190 | 98 | 116 | 191 |
| Residual & Reserve Propellant | 23 | 72 | 108 | 104 | 129 |
| Boil-Off | -- | -- | -- | 30 | 280 |
| Engine Weight | 200 | 100 | 270 | 270 | 270 |
| Power Supply Weight | 3000 | 2000 | -- | -- | -- |
| Propellant Weight | 1164 | 3587 | 5384 | 5188 | 6165 |
| Payload Weight | 4840 | 2271 | 2360 | 2512 | 1185 |

ION ENGINE EFFICIENCY

FIG.I

50
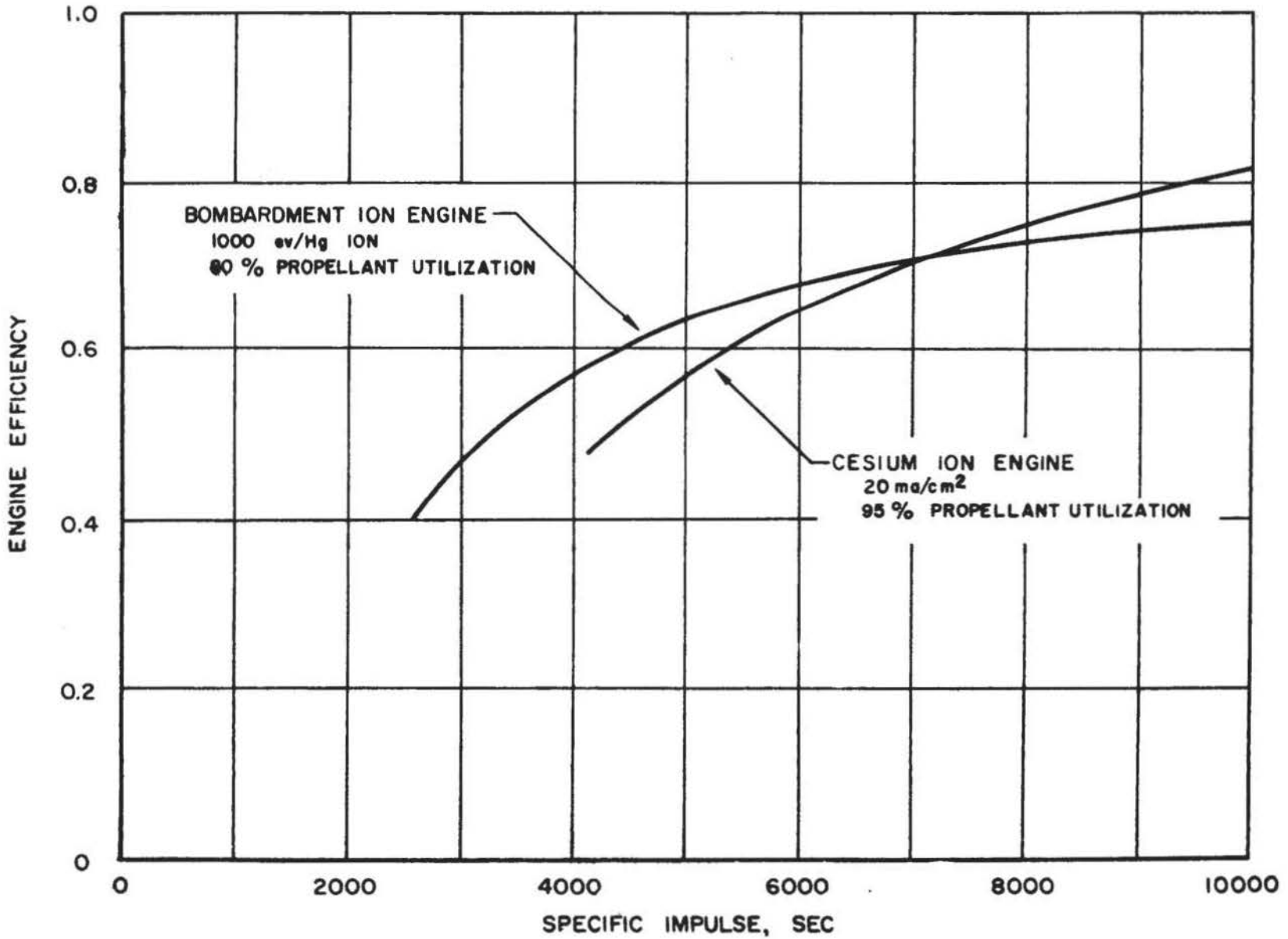
# ARC-JET ENGINE EFFICIENCY
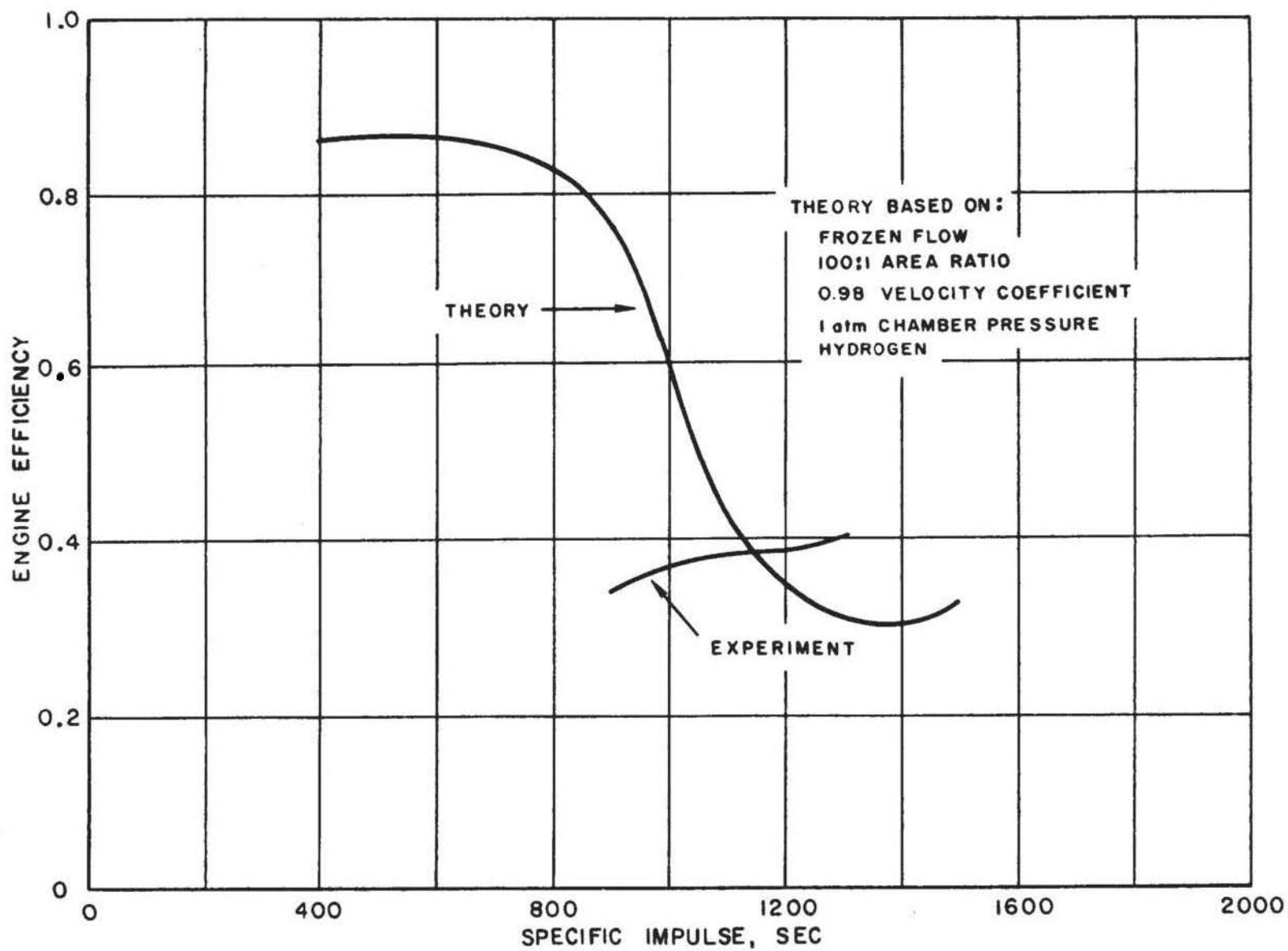
FIG. 2

# ENGINE EFFICIENCY SUMMARY
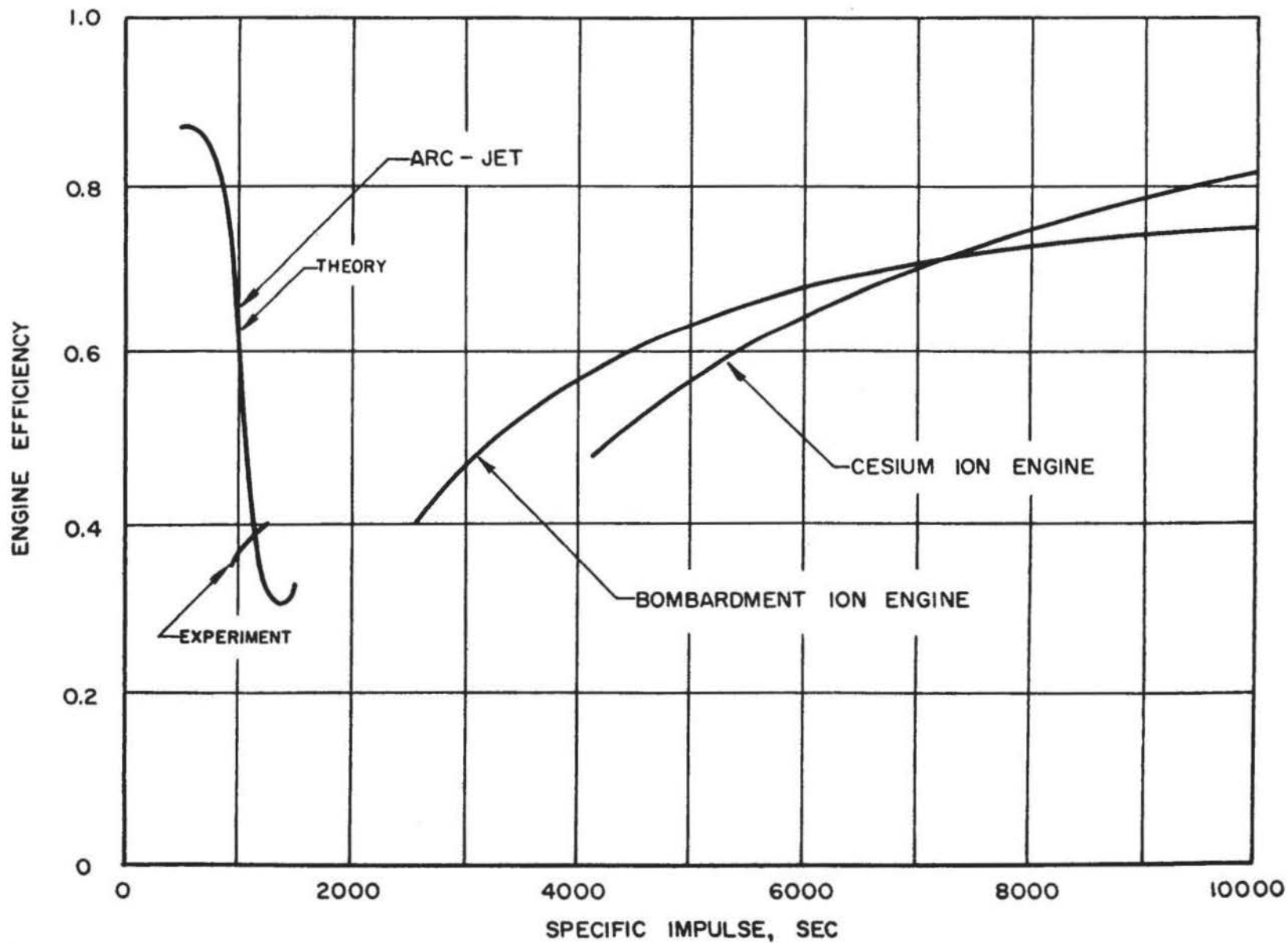
FIG. 3

# 24-HOUR EQUATORIAL SATELLITE MISSION
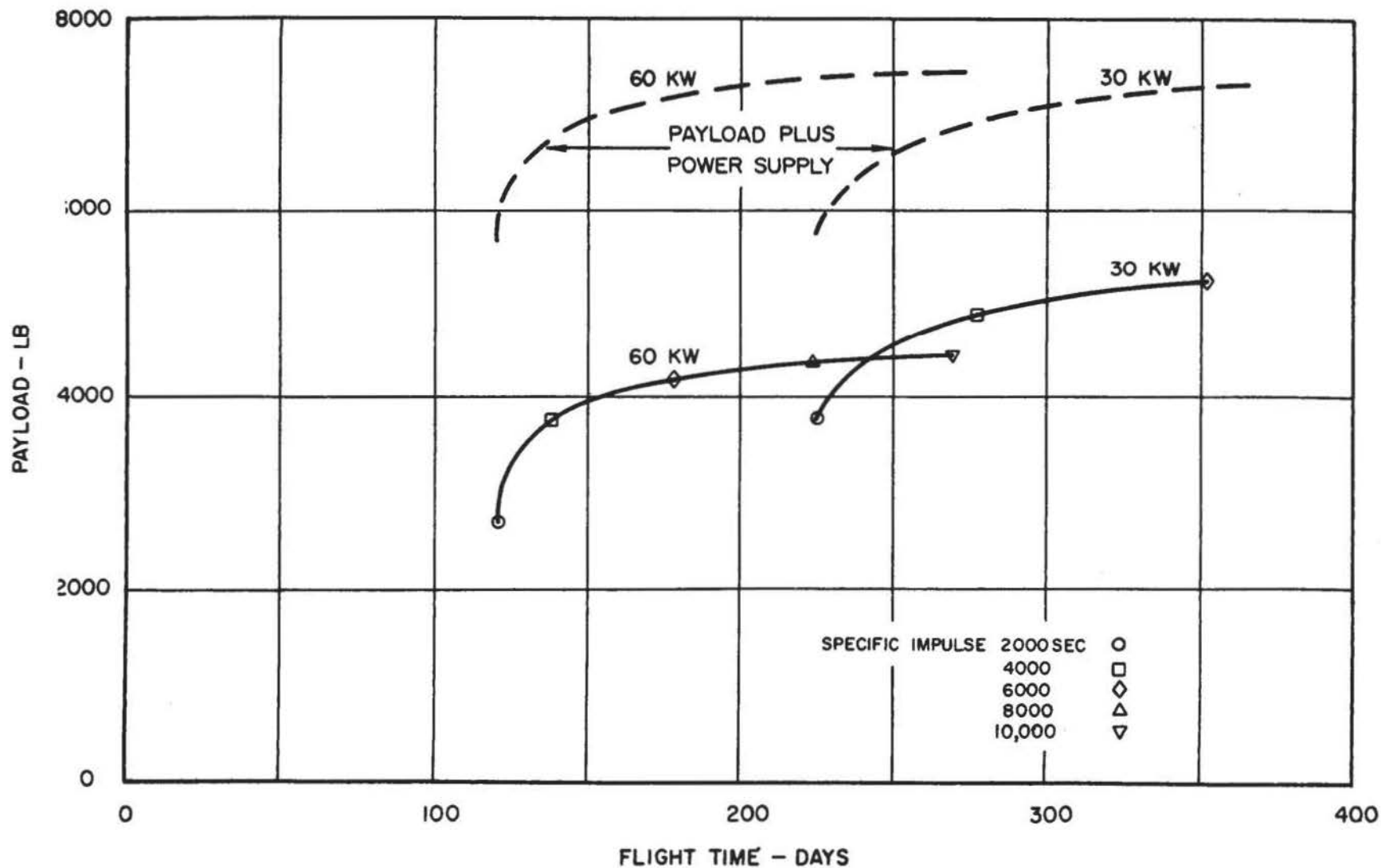
## BOMBARDMENT ION ENGINE          SNAP - 8

FIG. 4

FLIGHT TIME — DAYS

# 24 - HOUR EQUATORIAL SATELLITE MISSION

ION ENGINES                    SNAP - 8

FIG. 5

FLIGHT TIME – DAYS
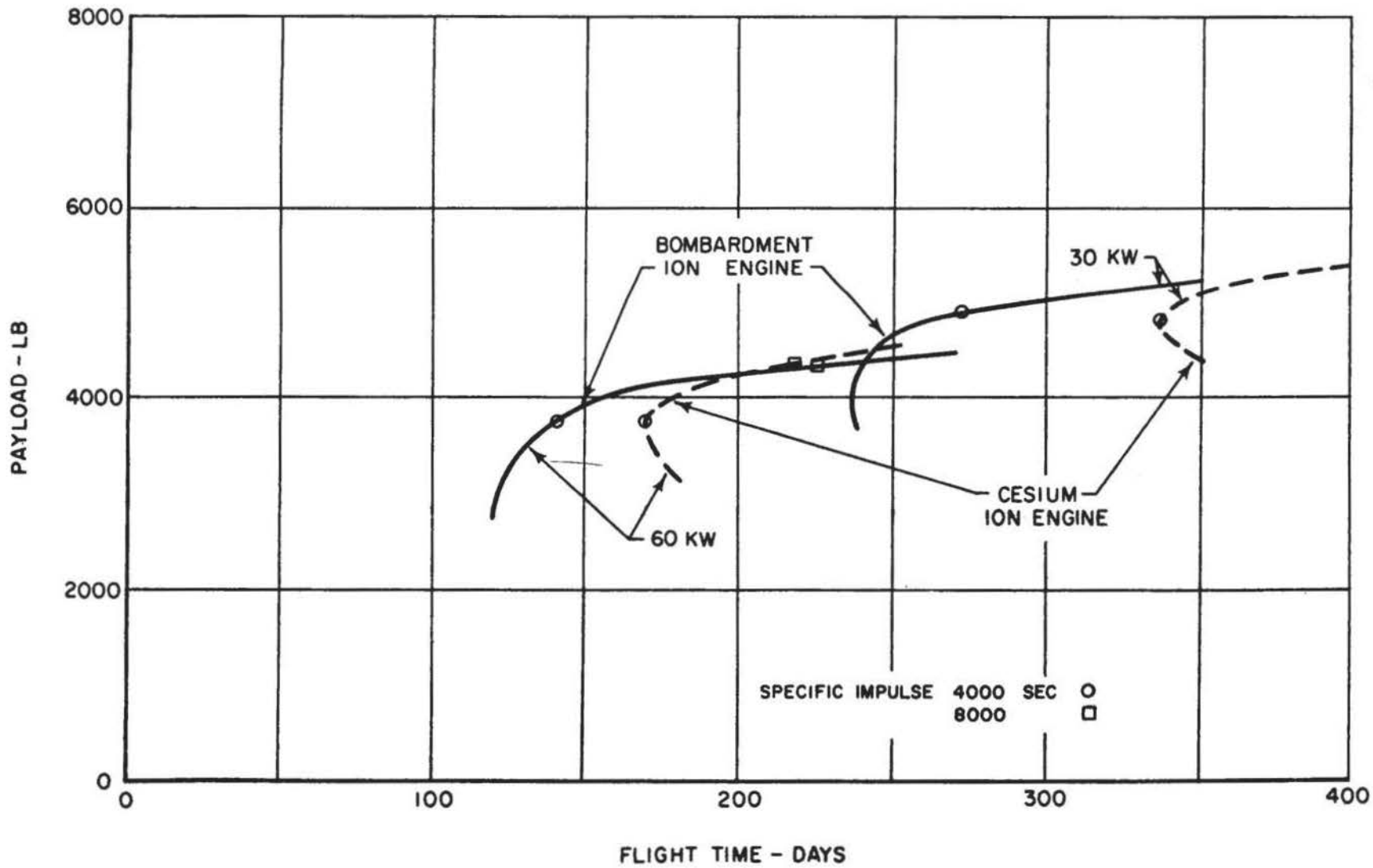
24-HOUR EQUATORIAL SATELLITE MISSION

60 KW          SNAP-8

ION ENGINE
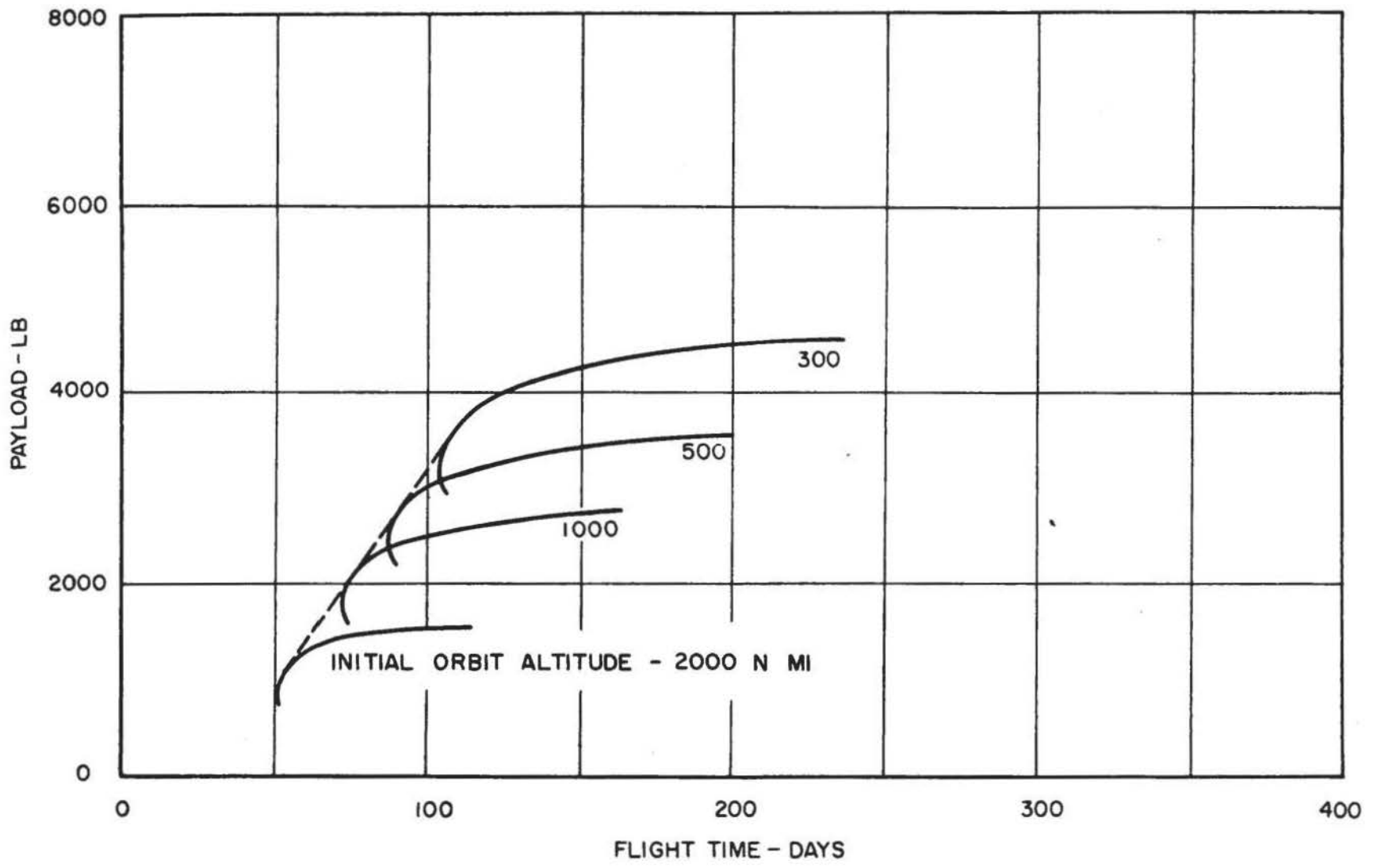
FIG. 6

24-HOUR EQUATORIAL SATELLITE MISSION

30 KW        SNAP-8

ION ENGINE
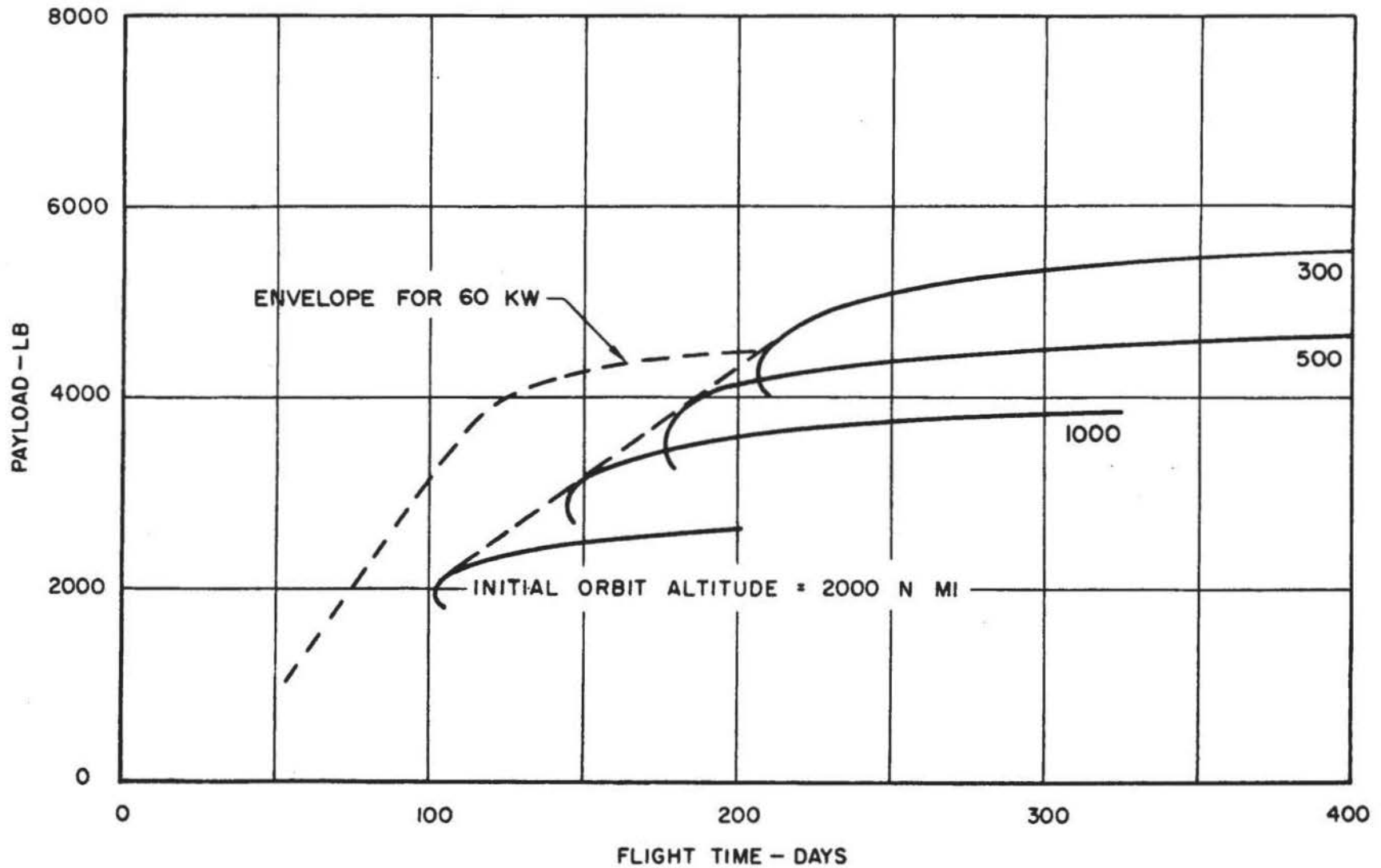
FIG. 7

# 24-HOUR EQUATORIAL SATELLITE MISSION
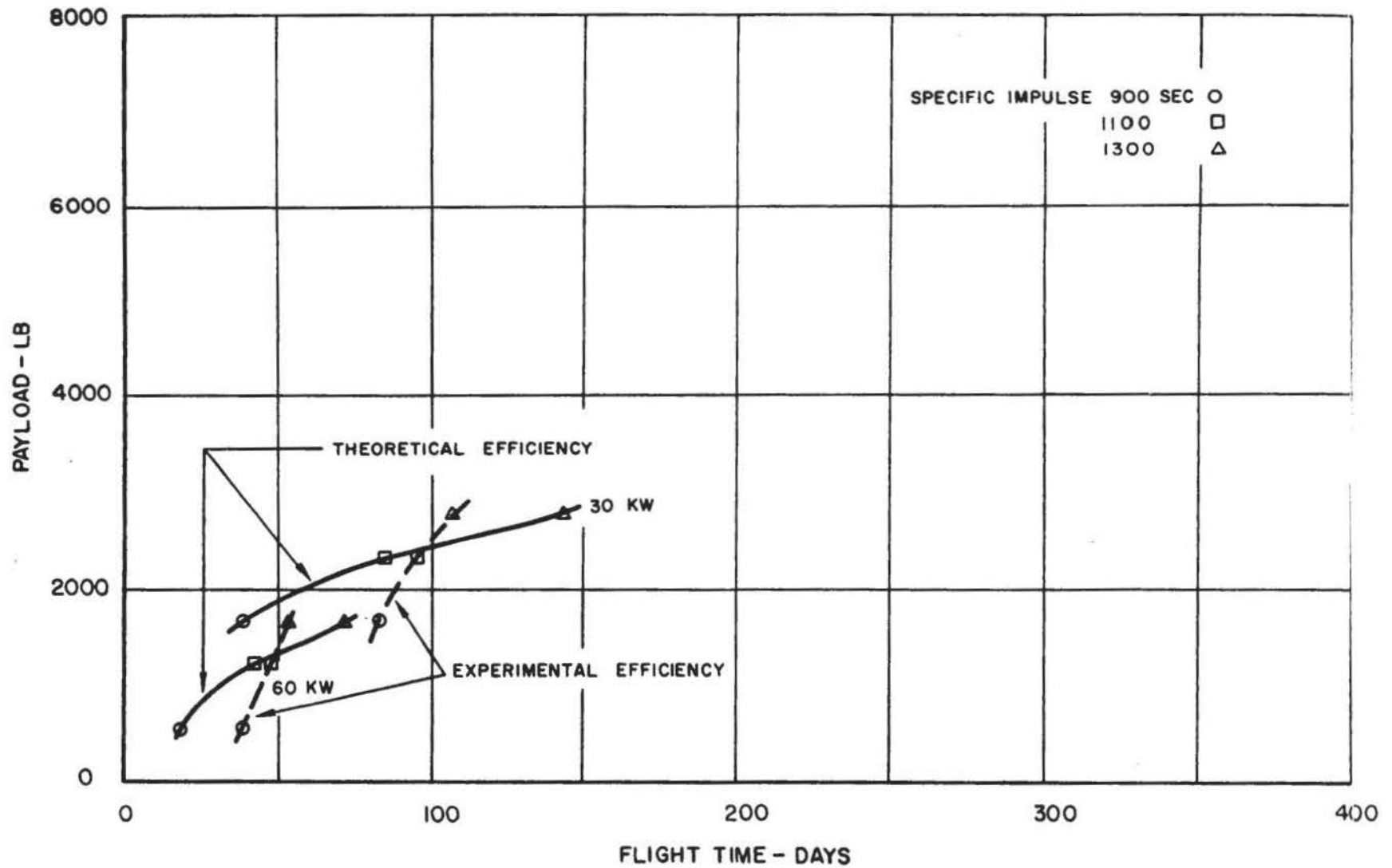
## ARC-JET ENGINE    SNAP-8

FIG. 8

# 24 - HOUR EQUATORIAL SATELLITE MISSION

## SNAP - 8

PAYLOAD - LB

FLIGHT TIME - DAYS

30 KW

60 KW

ION ENGINE

30 KW

ARC-JET ENGINE

60 KW
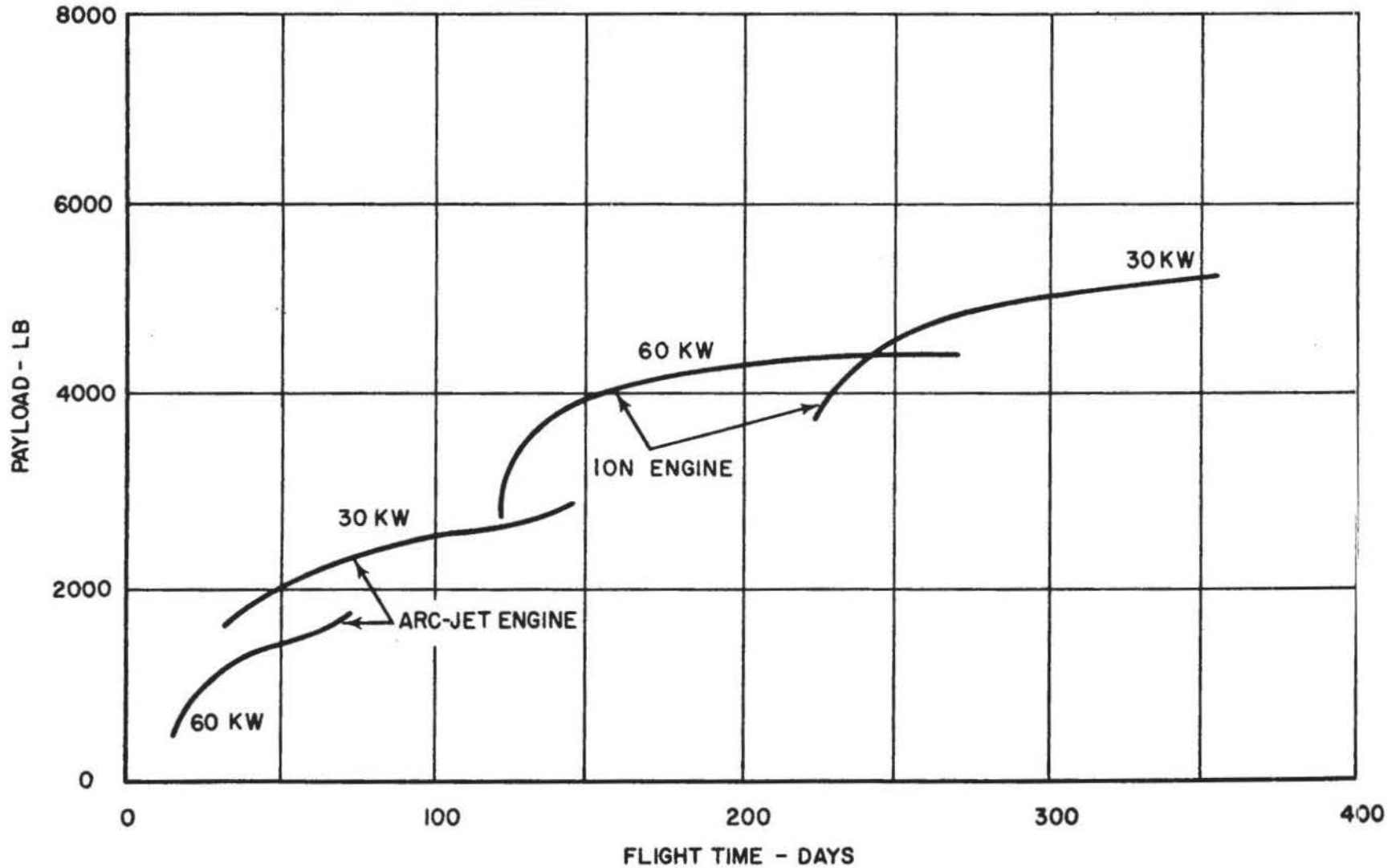
FIG. 9

# 24 - HOUR EQUATORIAL SATELLITE MISSION

## SNAP - 8

FLIGHT TIME – DAYS
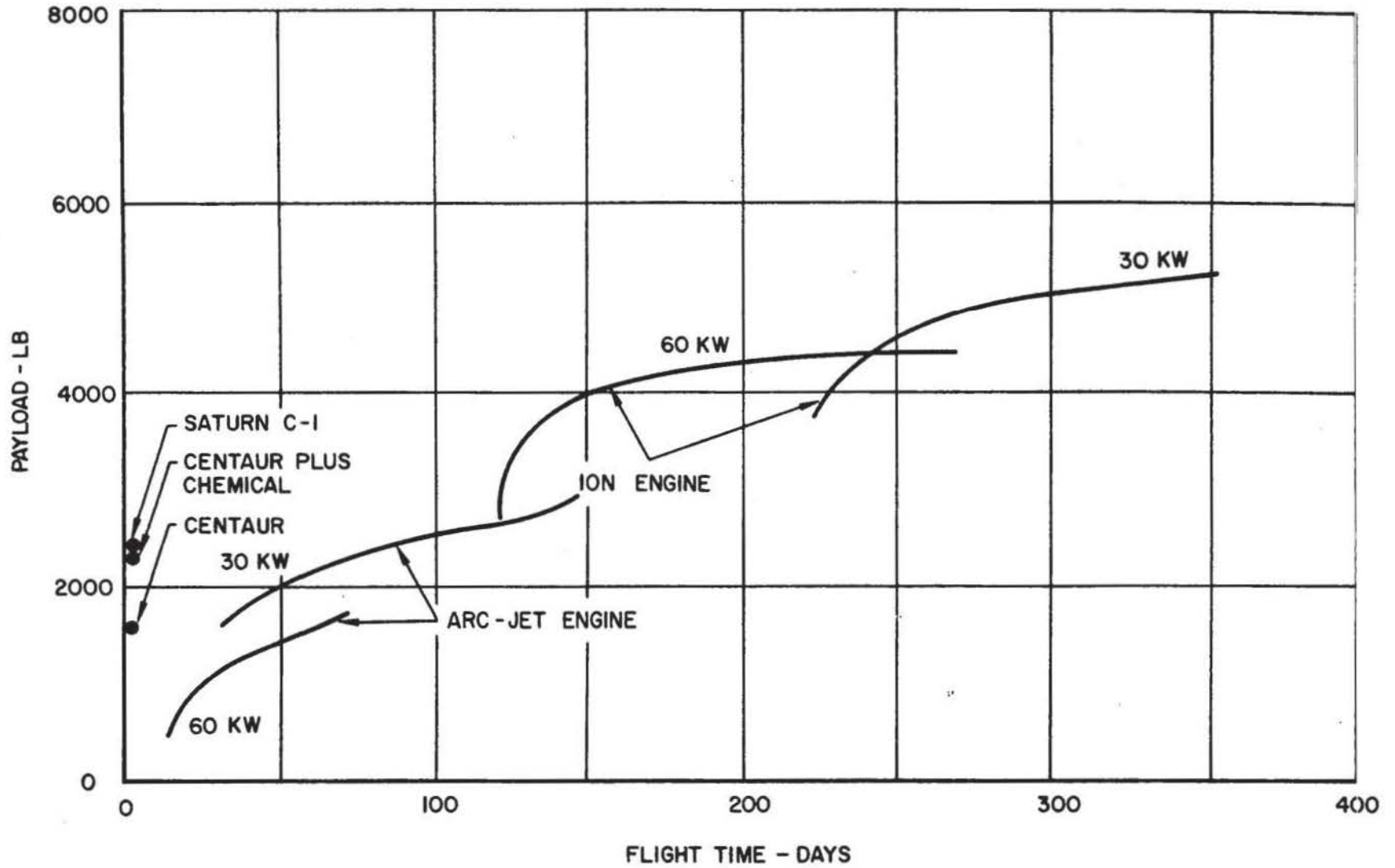
FIG. 10

# LUNAR SATELLITE MISSION

## BOMBARDMENT ION ENGINE      SNAP-8
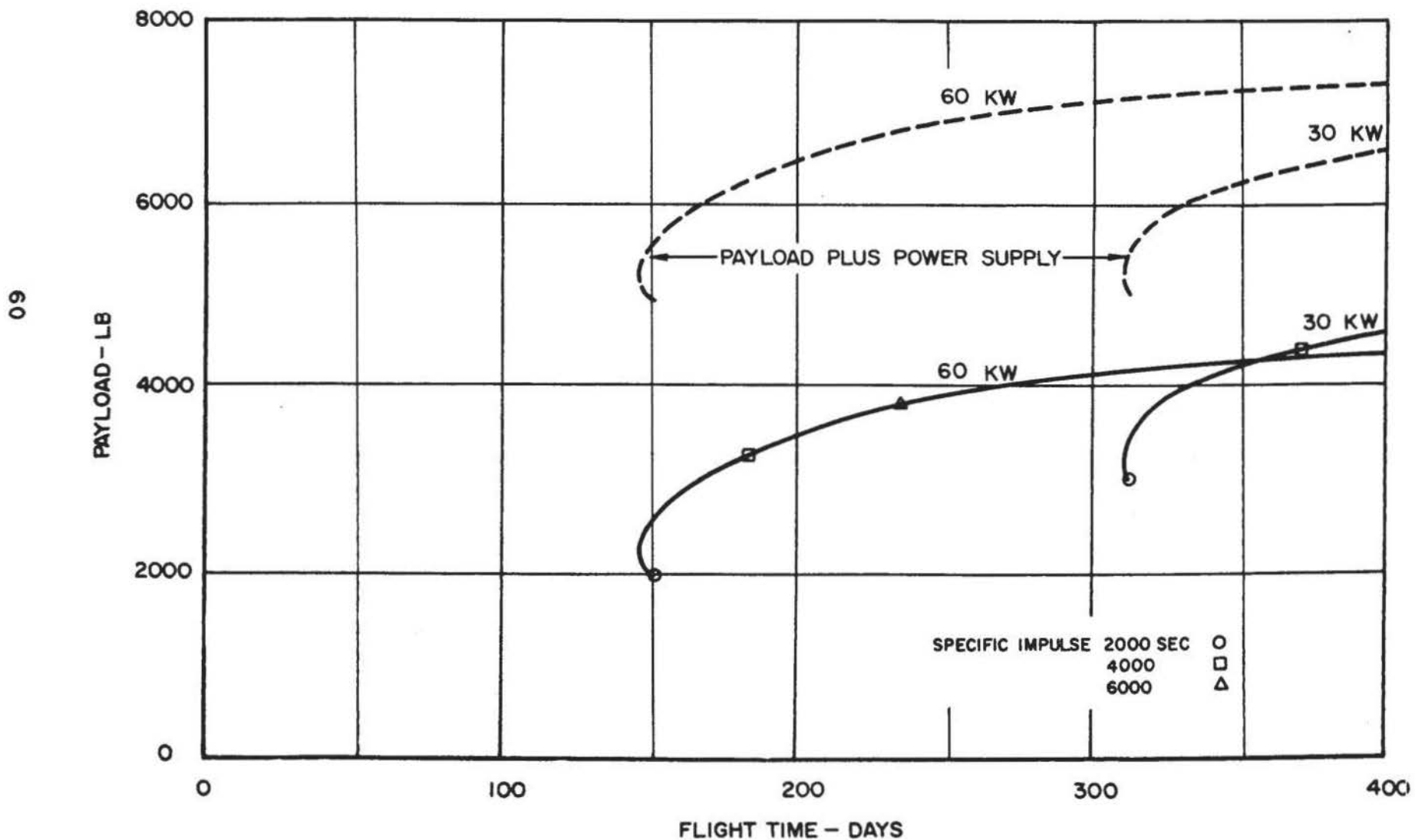


FIG. 11

# LUNAR SATELLITE MISSION

## ARC—JET ENGINE    SNAP—8
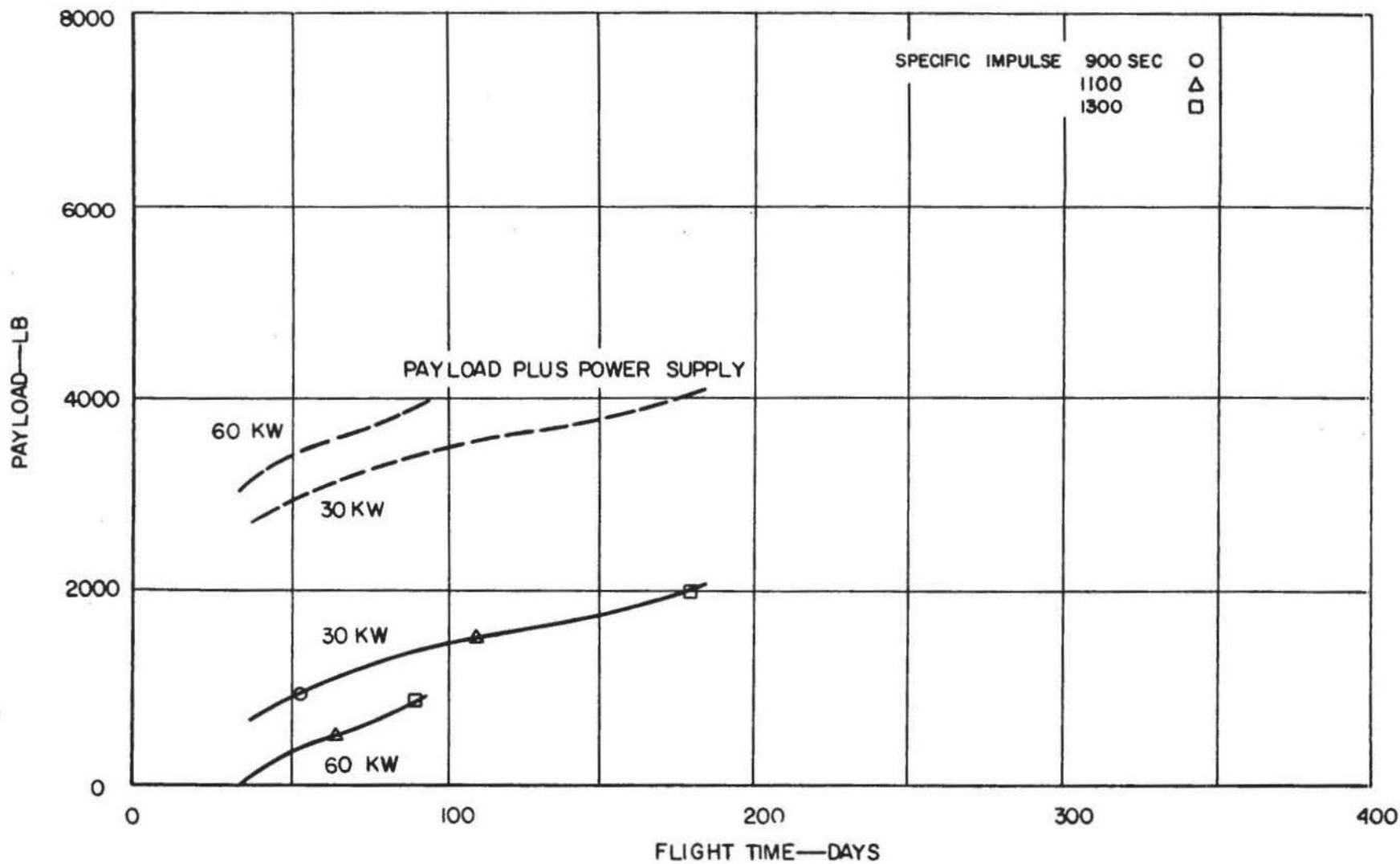
FIG. 12

# LUNAR SATELLITE MISSION
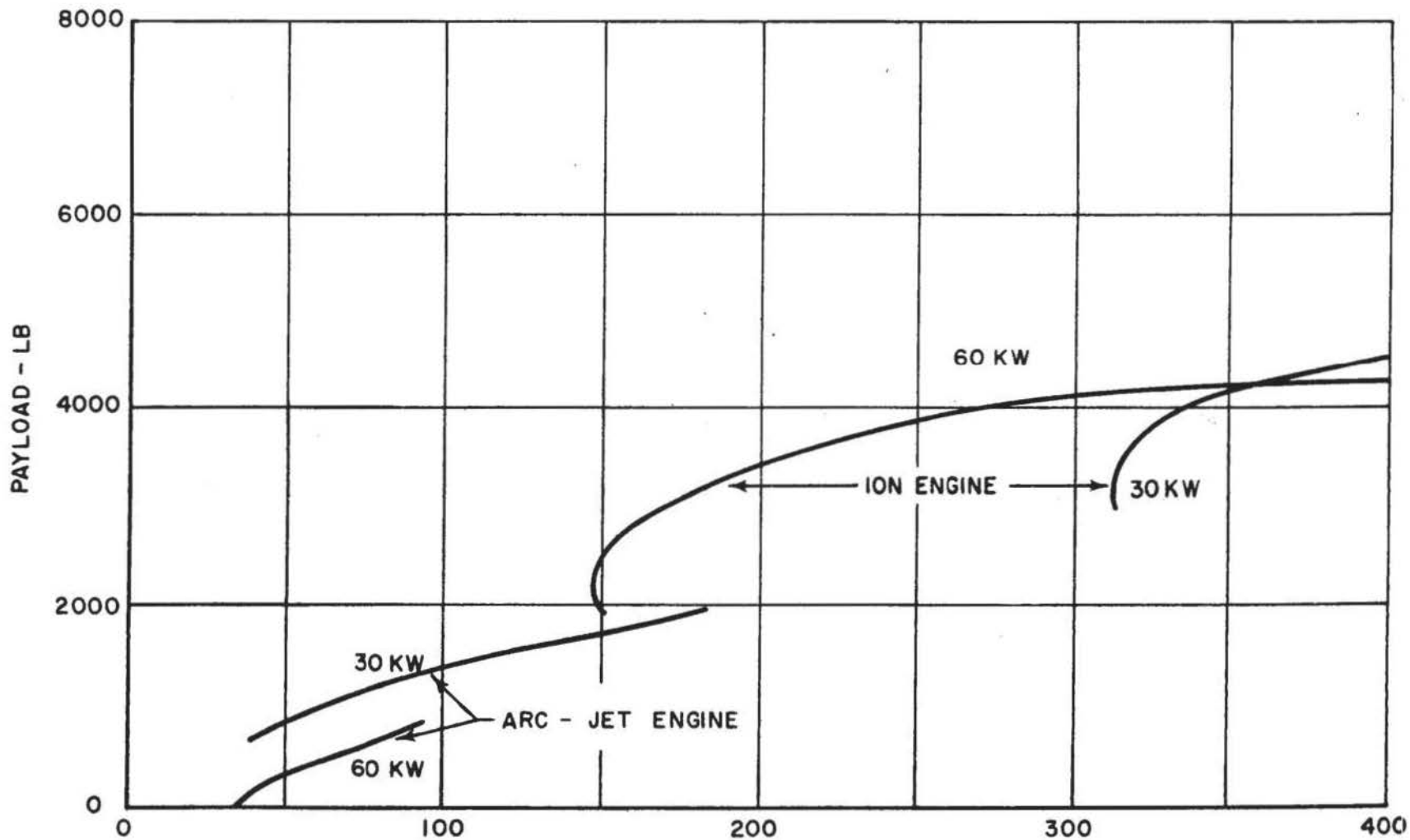
## SNAP-8

FIG. 13

# LUNAR SATELLITE MISSION
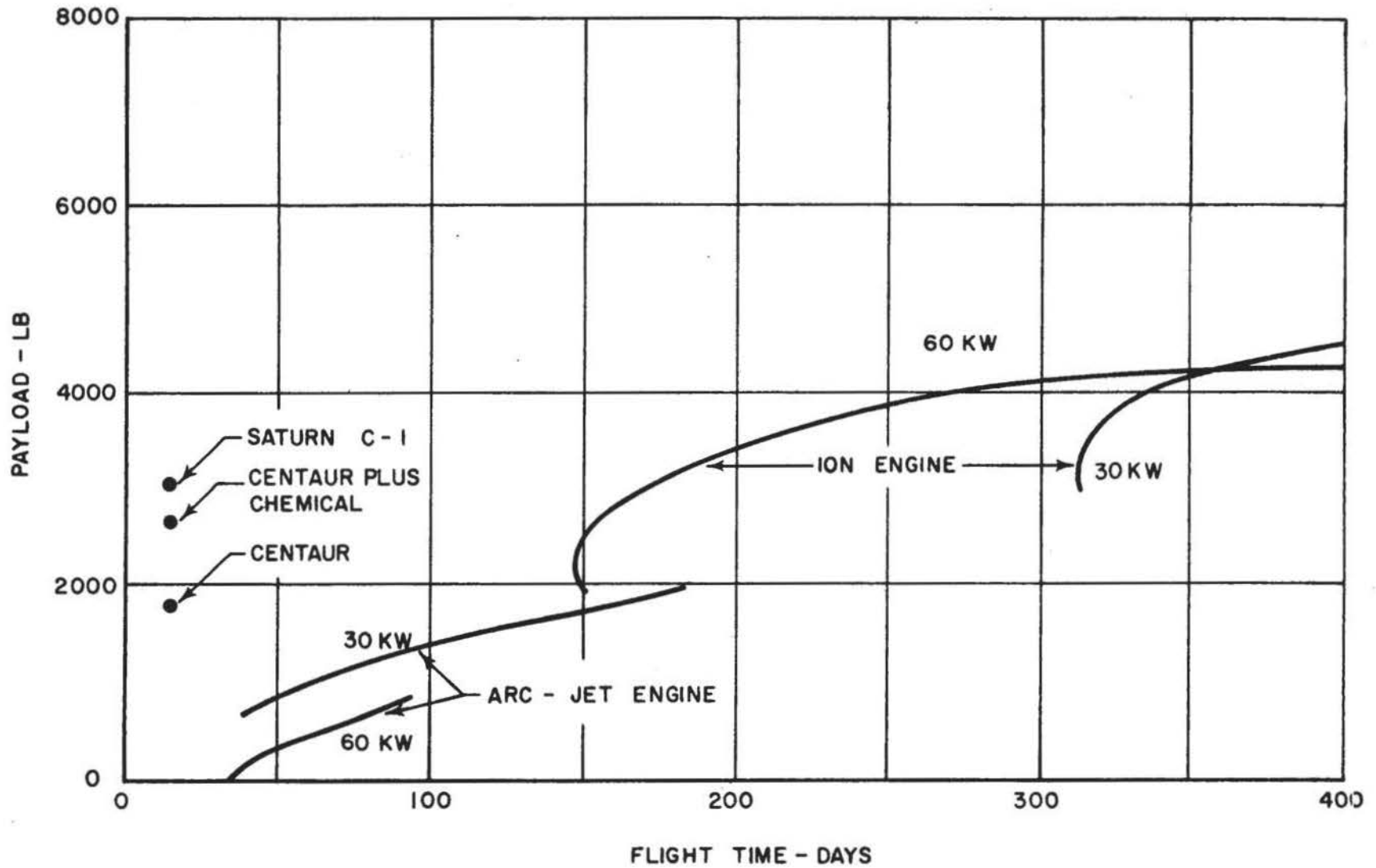
## SNAP-8

FIG. 14

# MARS SATELLITE MISSION

## BOMBARDMENT ION ENGINE    SNAP-8
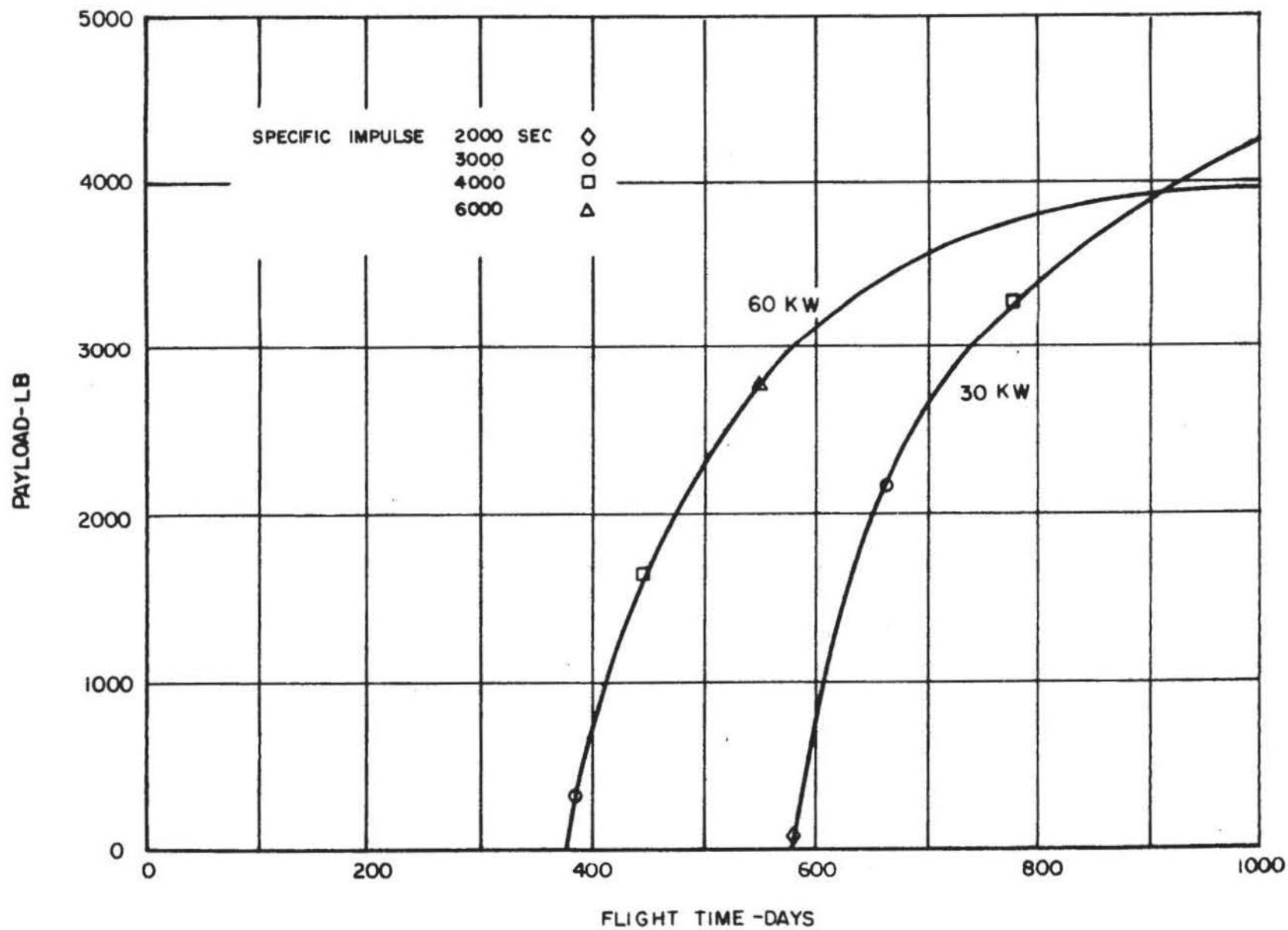
FIG. 15

# MARS SATELLITE MISSION
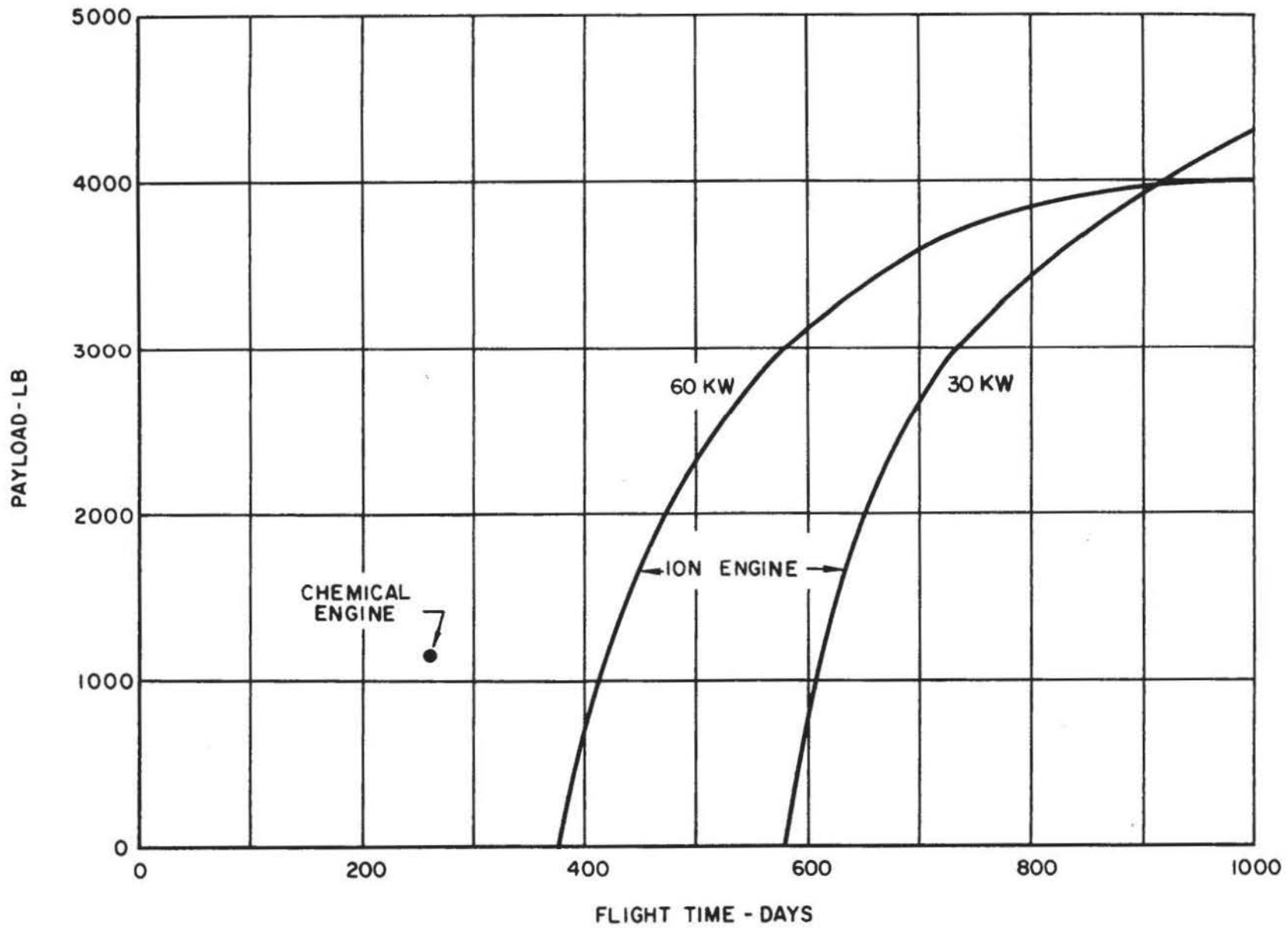
## SNAP-8

FIG. 16

# MERCURY PROBE MISSION

## BOMBARDMENT ION ENGINE

## 60 KW SNAP 8

FIG. 17

LAUNCH DATE - 1968
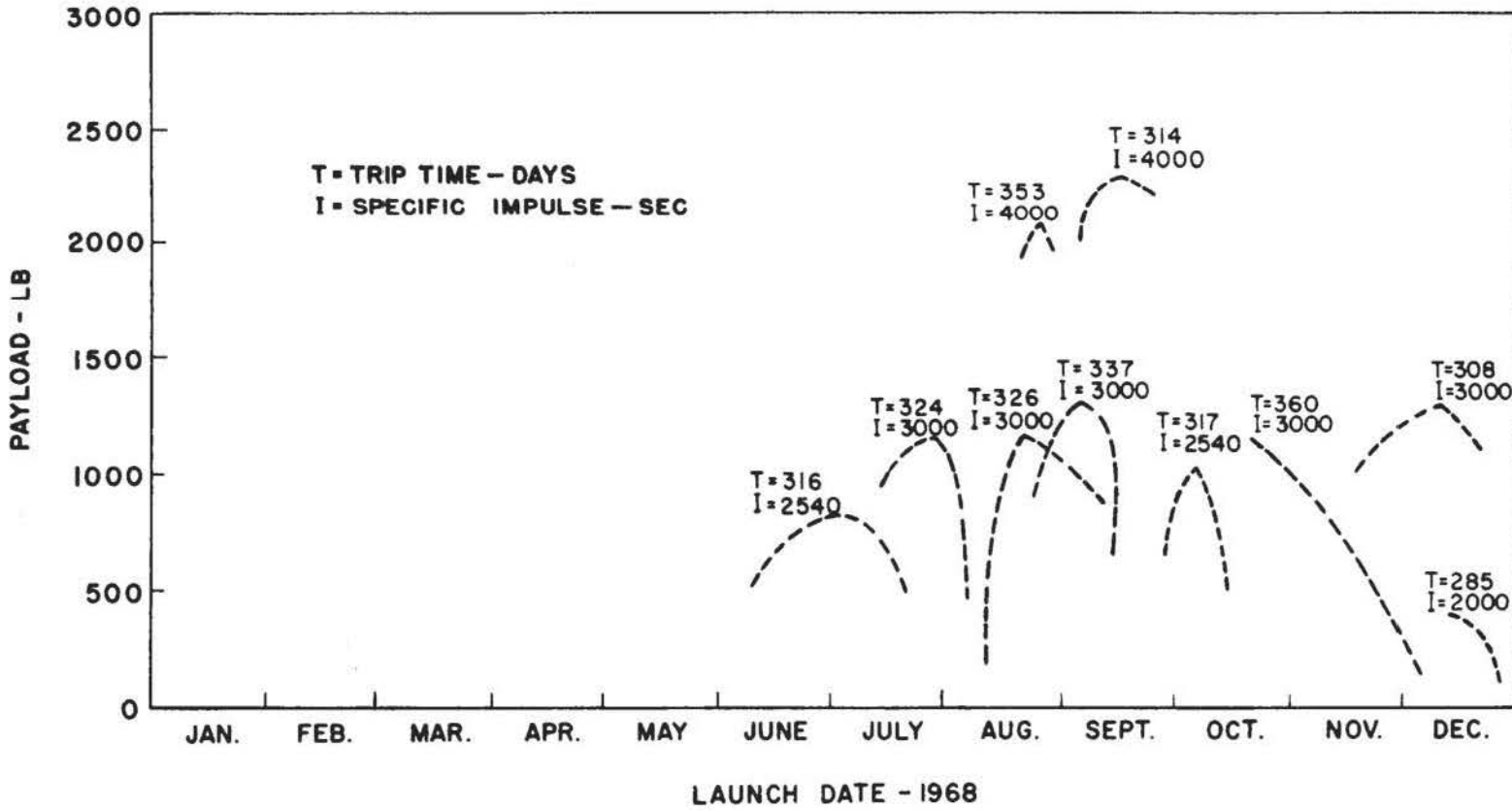
# MERCURY PROBE MISSION

## HYDROGEN-OXYGEN CHEMICAL ROCKET
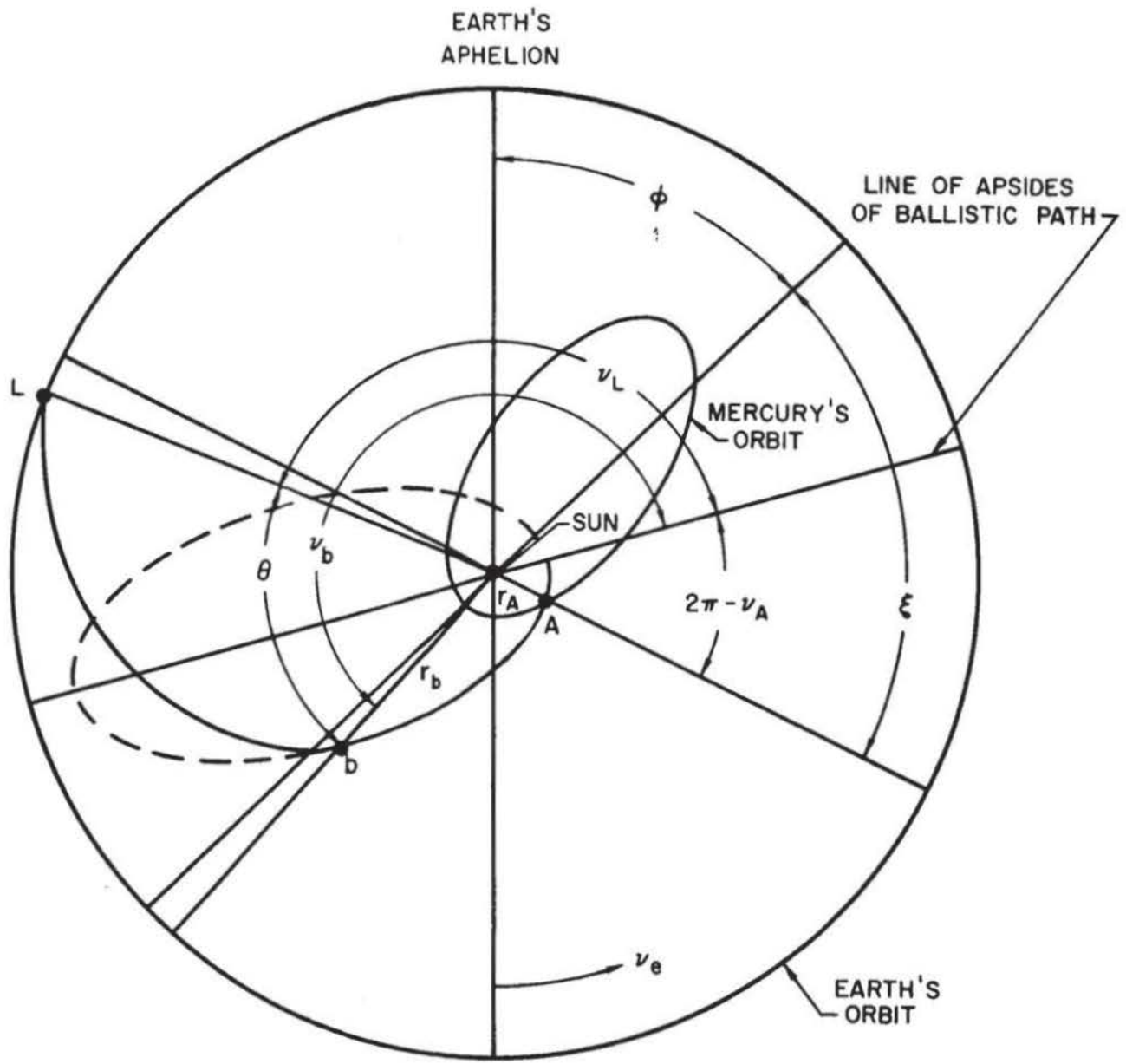


FIG. 18
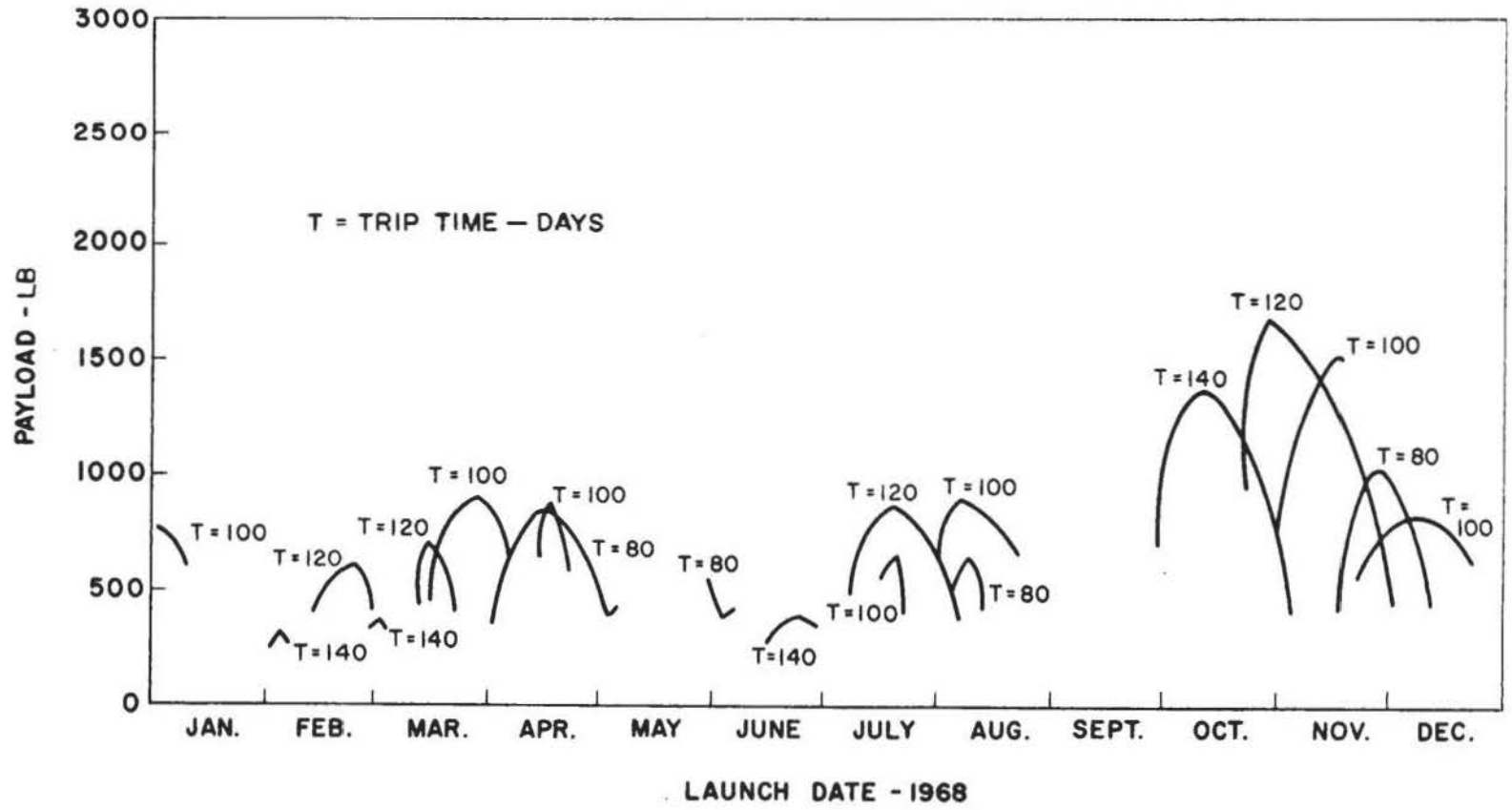
# MERCURY PROBE MISSION
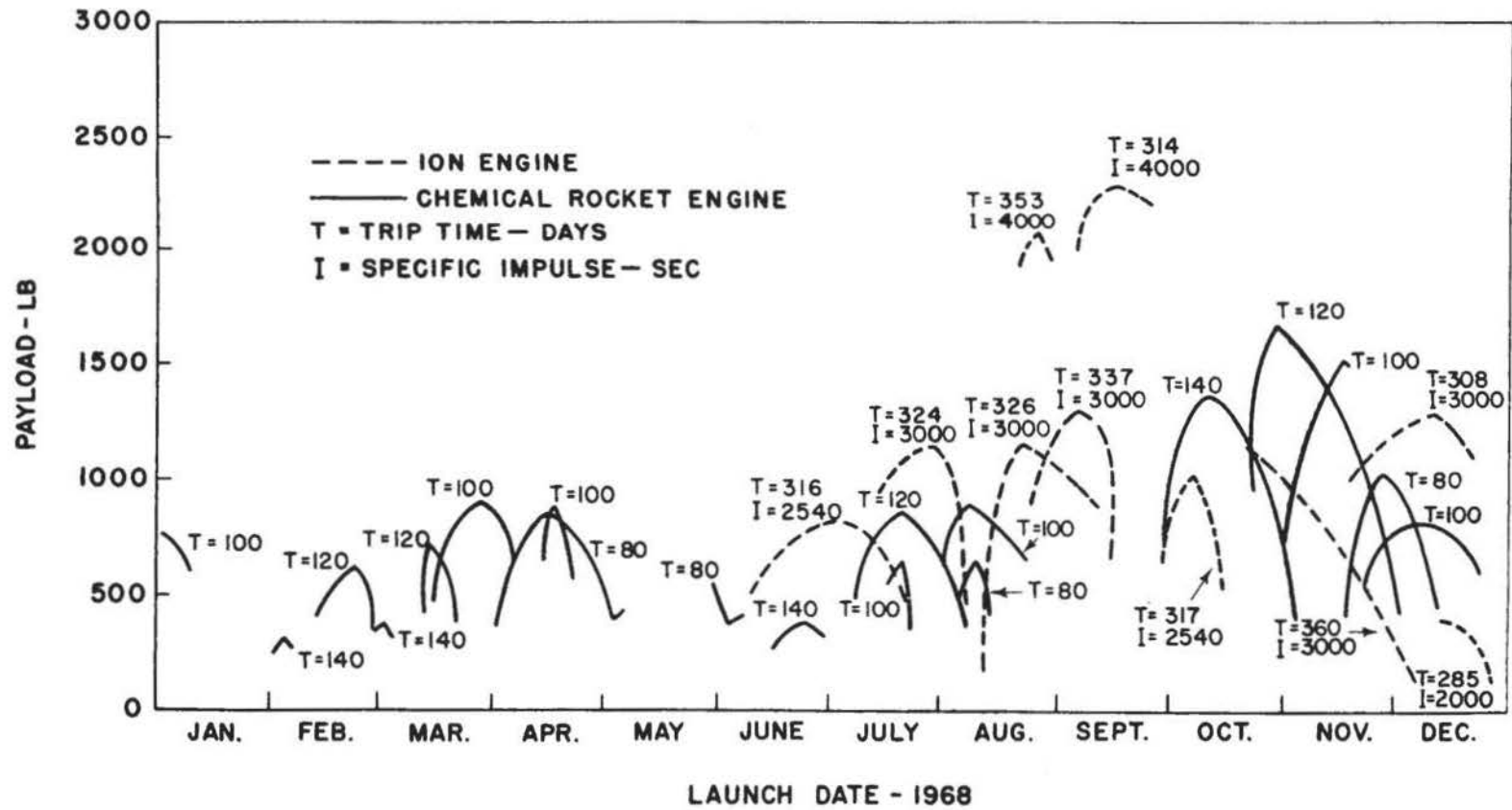
FIG. 19

# OUT-OF-ECLIPTIC MISSION

## 15 DEGREE CELESTIAL LATITUDE
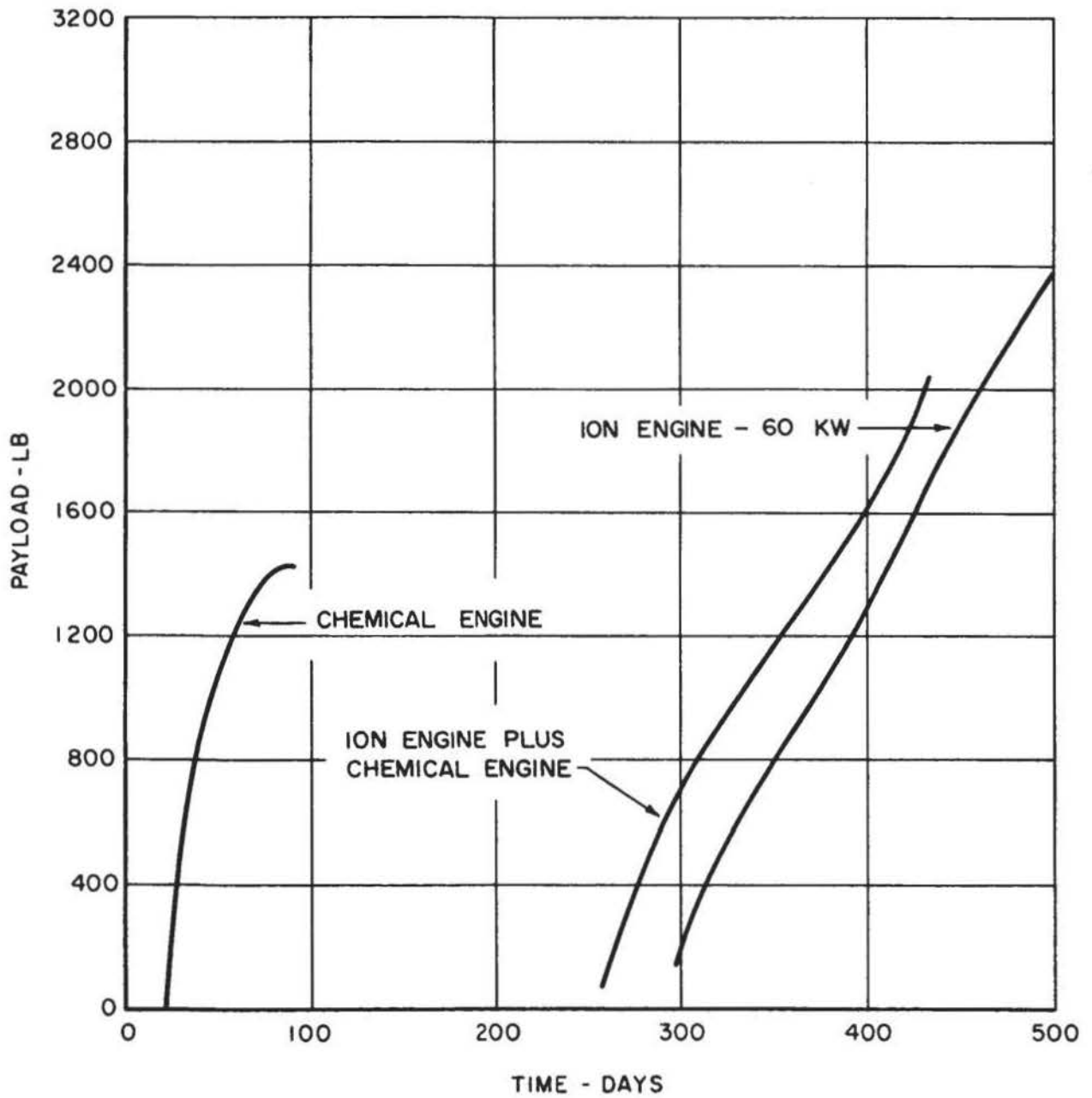
# PLANAR GEOMETRY OF LOW-THRUST MERCURY PROBE MISSION



L-b POWERED PHASE
b-A BALLISTIC PHASE

# EFFECTS OF TRANSFER ORBIT INCLINATION ON THREE DIMENSIONAL SYSTEM GEOMETRY FOR LOW-THRUST MERCURY PROBE MISSION



L-b POWERED PHASE
b-A BALLISTIC PHASE

EARTH'S PERIHELION

SHADED PORTION OF BALLISTIC ORBIT IS BELOW THE ELLIPTIC

FIG. 23
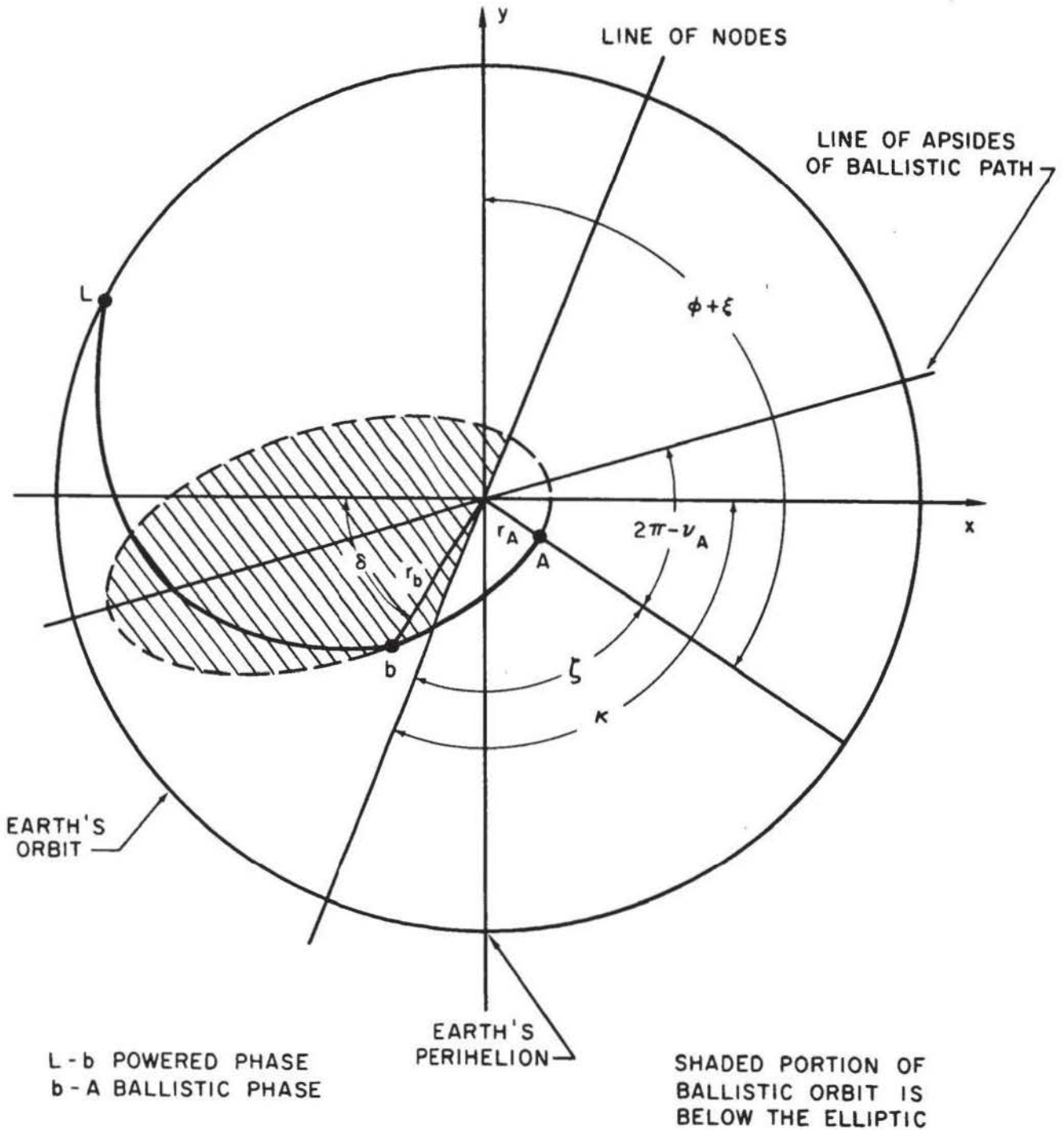
# VEHICLE LAYOUT FOR INSULATION SYSTEM ANALYSIS
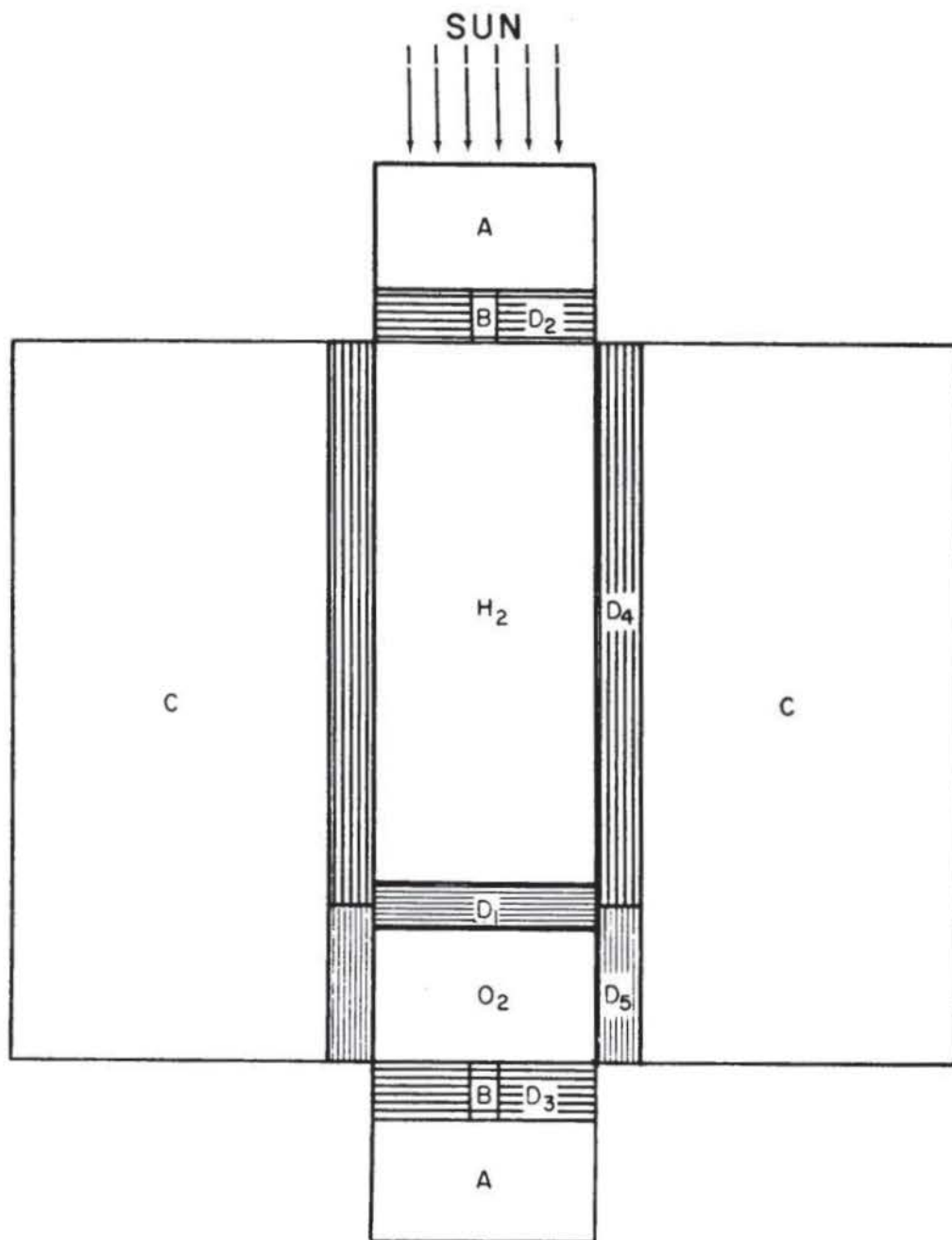


A  CONSTANT-TEMPERATURE HEAT SOURCES

B  THERMAL CONDUCTION PATHS

C  HEAT RADIATOR FOR POWER SUPPLY

D  REFLECTIVE FOIL SURFACES
   1    INTERFACE
   2,3  ENDS
   4,5  CYLINDERS